HAL open science

Spatio-temporal analysis of strawberry architecture: insights into the control of branching and inflorescence complexity

Marc Labadie, Karine Guy, Marie-Noëlle Demené, Yves Caraglio, Gaetan Heidsieck, Amélia Gaston, Christophe Rothan, Yann Guédon, Christophe Pradal, Béatrice Denoyes

To cite this version:

Marc Labadie, Karine Guy, Marie-Noëlle Demené, Yves Caraglio, Gaetan Heidsieck, et al.. Spatio-temporal analysis of strawberry architecture: insights into the control of branching and inflorescence complexity. Journal of Experimental Botany, 2023, 74 (12), pp.3595-3612. 10.1093/jxb/erad097 . hal-04084880

HAL Id: hal-04084880

https://hal.inrae.fr/hal-04084880v1

Submitted on 28 Apr 2023

HAL is a multi-disciplinary open access archive for the deposit and dissemination of scientific research documents, whether they are published or not. The documents may come from teaching and research institutions in France or abroad, or from public or private research centers.

L'archive ouverte pluridisciplinaire **HAL**, est destinée au dépôt et à la diffusion de documents scientifiques de niveau recherche, publiés ou non, émanant des établissements d'enseignement et de recherche français ou étrangers, des laboratoires publics ou privés.

Distributed under a Creative Commons Attribution 4.0 International License

Spatio-temporal analysis of strawberry architecture: insights into the control of branching and inflorescence complexity

Marc Labadie[1,2], Karine Guy[3], Marie-Noëlle Demené[3], Yves Caraglio[4], Gaetan Heidsieck[1, 2], Amelia Gaston[1], Christophe Rothan[1], Yann Guédon[2 ♀], Christophe Pradal[2,5*], and Béatrice Denoyes[1*]

[1]Univ. Bordeaux, INRAE, Biologie du Fruit et Pathologie, UMR 1332, F-33140, France

[2]CIRAD, UMR AGAP Institut, F-34398 Montpellier, France

[3]INVENIO, MIN de Brienne, 110 quai de Paludate, 33800 Bordeaux, France

[4]CIRAD, UMR AMAP and Université de Montpellier, 34398 Montpellier, France

[5]Inria & LIRMM, Univ Montpellier, CNRS, Montpellier, France

[♀]Deceased

[*]Authors for correspondence:

Béatrice Denoyes; Email: beatrice.denoyes@inrae.fr; ORCID 0000-0002-0369-9609

Christophe Pradal; Email: christophe.pradal@cirad.fr; ORCID 0000-0002-2555-761X

Accepted Manuscript

© The Author(s) 2023. Published by Oxford University Press on behalf of the Society for Experimental Biology.

This is an Open Access article distributed under the terms of the Creative Commons Attribution License (https://creativecommons.org/licenses/by/4.0/), which permits unrestricted reuse, distribution, and reproduction in any medium, provided the original work is properly cited.

Downloaded from https://academic.oup.com/jxb/advance-article/doi/10.1093/jxb/erad097/7143673 by INRAE Institut National de Recherche pour l'Agriculture, l'Alimentation et l'Environnement user on 28 April 2023

Highlight:

Here, we propose the open-source OpenAlea.Strawberry software combining 2D and 3D representations and statistical methods to explore the genetic diversity and spatio-temporal evolution of plant architecture in cultivated strawberry.

Accepted Manuscript

Downloaded from https://academic.oup.com/jxb/advance-article/doi/10.1093/jxb/erad097/7143673 by INRAE Institut National de Recherche pour l'Agriculture, l'Alimentation et l'Environnement user on 28 April 2023

Abstract/Summary

Plant architecture plays a major role in flowering and therefore in crop yield. Attempts to visualize and analyze strawberry plant architecture have been scarce to date. Here, we propose an open-source software combining 2D and 3D representation of plant development over time and statistical methods to explore the variability in spatio-temporal development of plant architecture in cultivated strawberry. We applied this software to six seasonal strawberry varieties whose plants were exhaustively described monthly at the node scale. Results showed that the architectural pattern of the strawberry plant is characterized by a decrease of the module complexity between the zeroth-order module (primary crown) and higher-order modules (lateral branch crowns (BC) and extension crowns). Furthermore, for each variety, we could identify traits with a central role in determining yield such as date of appearance and number of branches. By modeling the spatial organization of axillary meristem fate on the zeroth-order module using a hidden hybrid Markov/semi-Markov mathematical model, we further identified three zones with different probabilities of production of BC, dormant buds or stolons. This open-source software will be precious for the scientific community and breeders to study the influence of environmental and genetic cues on strawberry architecture and yield.

Key words: *Fragaria* × *ananassa*, plant architecture, branching, hidden hybrid Markov/semi-Markov chain, OpenAlea, multiscale tree graph.

Accepted Manuscript

Downloaded from https://academic.oup.com/jxb/advance-article/doi/10.1093/jxb/erad097/7143673 by INRAE Institut National de Recherche pour l'Agriculture, l'Alimentation et l'Environnement user on 28 April 2023

Introduction

Plant architecture is one of the most important agronomic traits that determines yield in crops (Mathan *et al*., 2016). It is under genetic control (Reinhardt and Kuhlemeier, 2002; Wang and Li, 2006) and influenced by environmental conditions (Teichmann and Muhr, 2015). The final architecture of the plant and subsequently the yield depends on the ontogenetic dynamics of the apical and axillary meristems.

Plant architecture is defined as the spatial organization of the plant (Hallé and Oldeman, 1970). In a typical plant architecture, the shoot apical meristem (SAM) establishes the primary axis of the plant by initiating a succession of vegetative entities named phytomers. A phytomer represents the basic unit of the plant axis and consists of an internode and a node with its attached leaf and its axillary bud (AXB). From this primary axis, the apical meristem from the AXB, hereafter also named AXM, will lead to the formation of axillary productions (branch, flower…). In sympodial growth, the SAM becomes a flower or an inflorescence and growth is continued by one or more apical meristems from the AXBs, which repeat the process in secondary axes (Schmitz and Theres, 1999). While the axis is a succession of phytomers, the plant is a succession of axes, primary, secondary, tertiary…. In this plant, the module refers to a determinate axis (primary, secondary, tertiary…) edified by a single SAM. The linear succession of modules constitutes an apparent axis (Barthélémy and Caraglio, 2007). Because of the repetition of these growth and branching processes, plants can be formally described through rooted Multiscale Tree Graphs (MTG) whose vertices correspond to their constituting botanical entities and edges represent the physical connections between them (Godin and Caraglio, 1998). In this multiscale representation, the architecture can be described at phytomer and axis scales (Barthélémy and Caraglio, 2007) and visualized in 2D and 3D (Pradal *et al.*, 2009; Pradal and Godin, 2020).

Perennial plants differ from herbaceous annual plants by their architecture, notably for their branching habit (Schmitz and Theres, 1999). Architecture studies have been developed for annuals (e.g. rice, Chen *et al.,* 2020) and for woody perennials (Nicolini *et al*., 2003; Barthélémy *et al.*, 2009). These studies allowed the development of models for identifying ideotypes by correlating topology and yield capacity (e.g. in coffea, Cilas *et al.,* 2006). In herbaceous perennial model multiplied by seed, tomato is the main species studied (e.g. Safaa *et al*., 2009). In contrast, the architecture of herbaceous perennial models multiplied by vegetative propagation, such as strawberry, remains poorly known.

Cultivated octoploid strawberry (*Fragaria x annanassa)* is the main berry fruit crop in the Rosaceae family. Under production conditions, new tray plants (Fig. 1A), which are daughter-plants obtained through vegetative propagation in nursery, are planted each year. Fruit yield is determined by the intensity and duration of the flowering (Fig. 1B). Following the vegetative multiplication by stolon, which is a specialized and highly elongated stem, SAM activity produces a primary axis, named

Accepted Manuscript

Downloaded from https://academic.oup.com/jxb/advance-article/doi/10.1093/jxb/erad097/7143673 by INRAE Institut National de Recherche pour l'Agriculture, l'Alimentation et l'Environnement user on 28 April 2023

primary crown (PC) in strawberry (Fig. 1C). It consists of short internodes bearing adventitious roots, stipulated trifoliate leaves arranged in a rosette in spiral phyllotaxis of ⅖ (Savini *et al.*, 2006), axillary buds (AXB) containing AXMs and is terminated by an inflorescence. Its development is sympodial: after its PC has stopped growing, the strawberry plant continues its vegetative growth from the highest AXM of the crown, which produces an axis called extension crown (EC) (Fig. 1C) (Costes *et al.*, 2014). The originality of the strawberry plant is the fate of the other AXMs along the module (Tenreira *et al.*, 2017; Gaston *et al*., 2020) as they can develop either into lateral axes named lateral branch crown (BC) (Sugiyama *et al.*, 2004) or stolons, or stay dormant (Fig. 1C). Their fate, which is controlled by genetic and environmental factors (Tenreira et *al.*, 2017; Andrés *et al*., 2021; Gaston *et al.,* 2021), has direct impact on plant and fruit yield. To date, nothing is known about the spatial organization of these structural components and their temporal interdependencies. Indeed, the various attempts to visualize strawberry architecture by Guttridge (1955), and more recently by Savini *et al.* (2006) and Massenati *et al.* (2011), could not determine the fate of the different meristems of a strawberry plant according to spatial and temporal patterns.

The objective of this work was to explore and identify the variability in spatio-temporal development of plant architecture among contrasting seasonal genotypes of cultivated strawberry. As strawberry plants are bushy and compact, we chose to dissect subsets of plants. The dissection was done at successive dates during the seasonal production in order to understand the architectural development. The plant architecture was fully described at the phytomer and module scales and then encoded in the MTG. In order to achieve our objective, we design a pipeline of methods including plant description MTG encoded and various exploratory tools, visualization techniques, exploratory methods and statistical modeling approach. The modeling approach relies on hidden hybrid Markov/semi-Markov (HMSM) chains, a variant of hidden semi-Markov chains previously used to analyze branching patterns in many plant species (Guédon *et al*., 2022). Altogether, our results provide a new practical framework for strawberry architecture representation and analyses and, beyond, for modeling plant flowering and yield.

Materials and methods

Experimental protocol and datasets

Plant material and growth conditions

The five seasonal flowering varieties (Capriss, Ciflorette, Clery, Darselect and Gariguette) and the advanced line Cir107 of cultivated octoploid strawberry were studied in Labadie *et al*. (2019). The plants of the six varieties used in the experiment were produced at a single location in a nursery in Douville. For the six varieties, runners bearing daughter plants emerged in mid-June from the mother plants. The unrooted daughter plants were taken from the runners at the end of July, kept at 4°C in a climatic chamber for one week before being planted in trays containing a peat-based

Accepted Manuscript

Downloaded from https://academic.oup.com/jxb/advance-article/doi/10.1093/jxb/erad097/7143673 by INRAE Institut National de Recherche pour l'Agriculture, l'Alimentation et l'Environnement user on 28 April 2023

medium for rooting. For the six varieties, these plants, named tray plants, were placed side by side outdoors under shade and thus subjected to the same environmental conditions (Supplementary Fig. S1 for temperature and global radiation conditions). To meet chilling requirements, which differed between genotypes (Supplementary Table S1), the tray plants were placed in a climate chamber at 2°C at different dates in November until plantation in December. All the genotypes were planted on 10 December 2014 except Ciflorette (4 December) in soilless culture under tunnel into breeding ground bags (ORGAPIN) of 10L with drip irrigation and fertilization at a minimal temperature of 8°C. The tunnel was opened laterally when temperatures were above 18°C.

Architectural and morphological data

The architecture of nine plants per genotype was described approximately once per month at the same date in order to characterize the spatio-temporal development of the six genotypes from plantation (Fig. 1D) and to model their architecture (Figs 1E, 1F). The overall strategy is presented in Figure 2A. It should be noted that the architecture was described exhaustively at the phytomer, module and plant scale while the time sampling was rather scarce and the observation protocol consisted of plant dissection. This experimental protocol indeed favors the topological dimension with respect to the temporal dimension. The plant architecture was encoded in the MTG format (Fig. 1E; Fig. 2B; Supplementary Table S2 for details regarding the specification of this MTG). It defines the type of botanical entities (e.g. plant, axis, phytomer), their attributes and the type of relationship between elements (succession or branching). Each module contains a succession of phytomers with their type of axillary production (Fig. 2B). The order of a module corresponds to its branching order, *i.e.* the number of successive branching with zeroth-order (order 0) module for the primary crown (PC). We studied the three following types of axillary production: lateral branch crown (BC), which is a lateral extended axis with expanded leaves, stolon that is characterized by an elongated stem even at early stages of development, and dormant bud. Dormant buds are non-extended lateral axes in which leaf primordia are contained within the bud (Fig. 1C). For dormant buds, we described the developmental stage of their apical meristem (AXM) by binocular observation. The bud stage (Jahn and Dana, 1970) was classed into four categories: i) AB, aborted (meristem showing necrosis), ii) VB, vegetative (meristem dome is relatively flat), iii) IB, initiated (meristem dome raises above the developing stipules), and iv) FB, floral (from sepal development to emergence of inflorescence). The total number of flowers of each inflorescence was counted when inflorescence emerges. Extension crown (EC) (Fig. 1C) was not included in the description of axillary productions but was extracted when analyses were performed on the apparent axis.

Extraction of data at the module scale

To study the occurrence along time of successive branching modules according to the genotype, the frequency distribution of module orders was extracted from the MTG for six successive dates of observation (mid-December, early-January, mid-February, early-March, early-April, early-June) and for each genotype. Modules considered for the statistical analysis had an order up to the fourth order. This is due to the absence of fifth-order modules for Clery, Capriss and Cir107 and their low frequencies for the three other genotypes (1 for Gariguette, 3 for Ciflorette and 1 for Darselect). The

Accepted Manuscript

Downloaded from https://academic.oup.com/jxb/advance-article/doi/10.1093/jxb/erad097/7143673 by INRAE Institut National de Recherche pour l'Agriculture, l'Alimentation et l'Environnement user on 28 April 2023

only exception is the analysis of the dates of appearance of successive modules according to their orders. To study the composition of each module according to its order and genotype, the frequency distributions of the number of phytomers, number of flowers of the terminal inflorescence, and number of stolons were extracted for each module order and genotype by pooling all observation dates. These frequency distributions were explored and compared using standard statistical methods (e.g., ANOVA on ranks with post hoc tests for count variables) and graphical representations (Fig. 2B).

Extraction of data at the node scale

We investigated the homogenous zone of the axillary productions along the zeroth-order module and their sympodial axes using a hybrid Markov/semi-Markov model described hereafter. Sequences of axillary productions were extracted at the node scale along the apparent axis according to the rank of the phytomer along each module (Supplementary Table S3). The sample size was between 107 sequences of cumulative length 909 for Darselect and 212 sequences of cumulative length 1707 for Capriss.

3D and 2D visual exploration of the architecture

Two types of architectural visualization were designed: i) a 3D canopy exploration and ii) a 2D individual schematic representation based on the MTG within the *OpenAlea.Strawberry* Python package (see in Result section hereafter).

The schematic 3D visualization of the canopy (Fig. 2B) highlights the 3D spatial organization of the plant, including phyllotaxy. Vegetative development was represented using a color scale based on module order: zeroth-order (order 0, green color), first-order (order 1, red color), second-order (order 2, blue color), third-order (order 3, yellow color), fourth-order (order 4, purple color). The timing and intensity of flowering were indicated by modulating the size and shape of the light blue boxes representing the inflorescences (Fig. 2B).

The 2D schematic visualization (Fig. 1F; Fig. 2B) of the plant architecture is inspired from botanical sketches and highlights the sympodial branching as well as the different structures of the plant. The same representation was used for the axillary buds as in 3D. Inflorescences were visualized as a red rectangle. Axillary buds were represented by colored spheres according to their SAM stage. This 2D visualization allows summarized architectural patterns not visible in 3D such as type of axillary production that are not apparent in real looking 3D visualization due to the bushy habit of the strawberry and the apparent axis as a linear succession of modules.

Standardization procedure for selecting the most central individual for 2D schematic representation

Regarding the potential high structural complexity of the architecture and the small sample size, we chose to extract a representative individual for each observation date and each genotype. To this

Accepted Manuscript

Downloaded from https://academic.oup.com/jxb/advance-article/doi/10.1093/jxb/erad097/7143673 by INRAE Institut National de Recherche pour l'Agriculture, l'Alimentation et l'Environnement user on 28 April 2023

end, we ordered the 9 described plants within each sample from the most central to the most outlying using a robust standardized distance d_i based on few global variables $(x_{i,1}, \ldots, x_{i,j}, \ldots)$ (e.g., number of flowers, number of leaves, number of stolons, maximum module order and number of BC and EC):

$$d_i = \sum_j \frac{\left|x_{i,j} - \underline{x_j}\right|}{mad_j}$$

where $mad_j = \sum_i \left|x_{i,j} - \underline{x_j}\right|$ is the mean absolute deviation from the median $\underline{x_j}$ for the variable *j*.

Hidden hybrid Markov/semi-Markov chains to model axillary productions along apparent axis

The objective of our statistical modeling approach was to highlight a spatial organization of axillary productions. We based our statistical model on a hidden hybrid Markov/semi-Markow model (HMSM) (Guédon, 2005; Durand *et al*., 2005) (Fig. 2C). The sequences used for inferring the model were apparent axes extracted at the node scale from architectural data with two variables: the module order and its axillary productions. Module order is an instrumental variable to separate successive modules within the model. To this end, a HMSM was built for each genotype. A HMSM chain is a two-scale segmentation model whose aim is to segment apparent axes in successive modules and within zeroth-order modules in successive homogeneous axillary production zones. The model is defined by its states (Markovian and semi-Markovian), transition probabilities between states to model the succession of zones along the apparent axes, occupancy distributions to model the zone length in number of phytomers, and categorical observation distributions to model the axillary productions within a zone. Occupancy and categorical distributions are attached only to semi-Markovian states.

Hybrid Markov/semi-Markov chains can be defined as follows. Let $\{S_t\}$ be a hybrid Markov/semi-Markov chain with finite-state space $\{0, \ldots, J-1\}$. A *J*-state hybrid Markov/semi-Markov chain $\{S_t\}$ is defined by the following parameters:

- initial probabilities $\pi_j = P(S_1 = j)$ with $\sum_j \pi_j = 1$;
- transition probabilities
  - semi-Markovian state *i*: for each $j \neq i$, $p_{ij} = P(S_t = j | S_t \neq i, S_{t-1} = i)$ with $\sum_{j \neq i} p_{ij} = 1$ and $p_{ii} = 0$ by convention,
  - Markovian state *i*: $p_{ij} = P(S_{t-1} = i)$ with $\sum_j p_{ij} = 1$.

It should be noted that absorbing states (a state is said to be absorbing if, after entering this state, it is impossible to leave it) are necessarily Markovian.

Accepted Manuscript

Downloaded from https://academic.oup.com/jxb/advance-article/doi/10.1093/jxb/erad097/7143673 by INRAE Institut National de Recherche pour l'Agriculture, l'Alimentation et l'Environnement user on 28 April 2023

An explicit occupancy distribution is attached to each semi-Markovian state:

$$d_j(u) = P(S_{t+1} = j, S_t \neq j), \qquad u = 1,2, \dots$$

Since-$t = 1$ is assumed to correspond to a state entering, the following relation is verified:

$$P(S_t \neq j, S_{t-v} = j, v = 1, \dots, t) = d_j(t)\pi_j.$$

We define as possible parametric state occupancy distributions binomial distributions, Poisson distributions and negative binomial distributions with an additional shift parameter *d* (*d* ≥ 1) which defines the minimum sojourn time in a given state.

The binomial distribution with parameters *d*, *n* and *p* ($q = 1 - p$), B(*d*, *n*, *p*) where $0 \leq p \leq 1$, is defined by

$$d_j(u) = \binom{n-d}{u-d} p^{u-d} q^{n-u}, \qquad u = d, d+1, \dots, n.$$

The Poisson distribution with parameters *d* and *λ*, P(*d*, *λ*), where *λ* is a real number ($\lambda > 0$), is defined by:

$$d_j(u) = \frac{e^{-\lambda}\lambda^{u-d}}{(u-d)!}, \qquad u = d, d+1, \dots$$

The negative binomial distribution with parameters *d*, *r* and *p*, NB(*d*, *r*, *p*), where *r* is a real number (*r* > 0) and $0 < p \leq 1$, is defined by:

$$d_j(u) = \binom{u-d+r-1}{r-1} p^r q^{u-d}, \qquad u = d, d+1, \dots$$

A hidden hybrid Markov/semi-Markov chain (HMSM) (Guédon, 2005) can be viewed as a pair of stochastic processes $\{S_t, X_t\}$ where the "*output*" process $\{X_t\}$ is related to the "*state*" process $\{S_t\}$, which is a finite-state hybrid Markov/semi-Markov chain, by a probabilistic function or mapping denoted by *f* (hence $X_t = f(S_t)$). Since the mapping *f* is such that a given output may be observed in different states, the state process $\{S_t\}$ is not observable directly but only indirectly through the output process $\{X_t\}$. This output process $\{X_t\}$ is related to the hybrid Markov/semi-Markov chain $\{S_t\}$ by the observation (or emission) probabilities $b_j(y) = P(S_t = j)$. The definition of the categorical observation distributions expresses the assumption that the output process at time *t* depends only on the underlying hybrid Markov/semi-Markov chain at time *t*.

The maximum likelihood estimation of the parameters of a HMSM chain requires an iterative optimization technique, which is an application of the EM algorithm. Once a hybrid Markov/hidden semi-Markov chain has been estimated, the most probable state sequence can be computed for each observed sequence using the so-called Viterbi algorithm; see Guédon (2003, 2005, 2007) for the statistical methods for hybrid Markov/hidden semi-Markov chains. In our application context, the most probable state sequence corresponding to the zeroth-order module can be interpreted as

Accepted Manuscript

Downloaded from https://academic.oup.com/jxb/advance-article/doi/10.1093/jxb/erad097/7143673 by INRAE Institut National de Recherche pour l'Agriculture, l'Alimentation et l'Environnement user on 28 April 2023

the optimal segmentation of the corresponding observed sequence into successive axillary production zones.

In our context, the zeroth-order module is modeled as a chain of consecutive semi-Markovian states to decompose it in successive axillary production zones (states 0.1, 0.2 and 0.3 in Fig. 3A; distribution of axillary productions along the zeroth-order module in Fig. 3B). Higher order modules are modeled by an alternation of Markovian states corresponding to terminal inflorescences (states F0, F1, F2, F3 and F4 represented in Fig. 3A for the Ciflorette model) followed by a semi-Markovian state to represent homogeneous axillary production zone within a module (states 1, 2, 3, and 4 are semi-Markovian states in Fig. 3A).

For zeroth-order modules, the almost deterministic succession of states was used to assess the number of zones. We thus expected that the states stayed ordered and that the probabilities of skipping states were low as a byproduct of the iterative estimation procedure of a HMSM.

The maximum likelihood estimation procedure computes the parameters of the model, i.e. the probability of transition between two zones, the distribution of axillary productions for a given zone, and numbers of phytomers of a given zone. To this end, it uses an iterative optimization technique, which is an application of the Expectation–Maximization (EM) algorithm (Ephraim and Merhav, 2002). Once a HMSM has been estimated, the most probable state sequence can be computed for each observed sequence using the so-called Viterbi algorithm (Guédon, 2003; 2005; 2007). In our context, the most probable state sequence corresponding to the zeroth-order module can be interpreted as the optimal segmentation of the corresponding observed sequence into successive axillary production zones.

On the basis of the optimal segmentations of the observed sequences, model parameters were extracted for each genotype (Renton *et al*., 2006) in order to compare zeroth-order modules between genotypes on the basis of the global model estimated on the pooled sample.

Moreover, to have a global view of the dissimilarities between the axillary production patterns of the genotypes, we first compute the matrix of pairwise dissimilarities between HMSM chains using the Kullback–Leibler divergence, and then applied a hierarchical clustering approach on this matrix (Guédon *et al*., 2003). The dissimilarity measure is computed on generated axillary production sequences of fixed length, systematically starting with zeroth-order modules and ending with fourth-order modules. We also applied this approach to the comparison of the axillary production patterns of the genotypes restricted to the zeroth-order modules.

Accepted Manuscript

Downloaded from https://academic.oup.com/jxb/advance-article/doi/10.1093/jxb/erad097/7143673 by INRAE Institut National de Recherche pour l'Agriculture, l'Alimentation et l'Environnement user on 28 April 2023

Results

Spatio-temporal description of strawberry plant architecture using 3D and 2D representations

The strawberry plant has a compact structure (Fig. 1A), and therefore requires dissection to fully decipher its architecture. The terminal bud (TB) is located at the upper end of the primary crown (PC) and comprises the SAM and leaf primordia (Fig. 1C). The TB is surrounded by the petioles of developed leaves and is thus not visible on intact plants. The axillary buds (AXB) are located at the axil of each leaf and are only visible when leaves are removed. As shown in Fig. 1D, the AXB produces either a stolon, a lateral branch crown (BC), or remains dormant (a non-extended axis). A BC is a lateral axis comprising expanded leaves with an axillary meristem (AXM) at their axil and also an inflorescence under favorable conditions. Dissection of the AXB allows the characterization of its developmental stage according to the stage of its apical meristem (AXM) (Jahn and Dana, 1970; Gaston *et al*., 2021; see Materials and Methods). The meristem of a vegetative bud (VB) is vegetative. The meristem of an initiated bud (IB) is at the first stages of floral initiation (Fig. 1C) while the meristem of a flowering bud (FB) is at more advanced stages of flower and inflorescence development. Strawberry plant development is therefore viewed as a succession of incremental order modules (Fig. 1E). The zeroth-order module is the PC. Along this module, AXBs will produce either first-order modules (BC or extension crown, EC) or stolons, as shown in the 2D representation of the plant (Fig. 1F). BC and EC will produce higher order modules and stolons etc.

We reasoned that spatio-temporal variations in module-orders in cultivated strawberry (*Fragaria x ananassa*) should result in a diversity of plant architecture and flowering patterns and ultimately in yield patterns. To test this hypothesis, we studied six strawberry genotypes contrasting in plant architecture and fruit yield. The architecture was described exhaustively at the phytomer, module and plant scale levels using an experimental protocol that favors the topological dimension with respect to the temporal dimension. The plant architecture was encoded in the MTG format (Fig. 1E; Supplementary Table S2 for details regarding the specification of this MTG). It allowed us to obtain 2D (Fig. 1F) and 3D representations of the plant.

The 3D visualization of the canopy enabled the visual exploration of the reconstructed plants in order to determine the spatial organization, the flowering intensity and the phenology of the different genotypes (Fig. 4A for Ciflorette; Supplementary Figs S2, S3 for all genotypes). We can observe that at planting (mid-December) all the Ciflorette individuals consisted of zeroth- and first-order (green and red respectively) modules. Then, second-order (blue) modules appeared in mid-February. Third-order (yellow) and fourth-order (purple) modules appeared in early-May. Strikingly, the nine individuals of each genotype at each successive date of observation show a homogenous development, with similar module order distributions. When comparing all genotypes, we observed that they differed by their earliness of module development (Supplementary Fig. S2). For Gariguette, Clery and Ciflorette, first-order modules appeared in mid-February while they appeared in early-January for Capriss and Cir107 and in mid-December for Darselect. Second-order modules appeared

Accepted Manuscript

Downloaded from https://academic.oup.com/jxb/advance-article/doi/10.1093/jxb/erad097/7143673 by INRAE Institut National de Recherche pour l'Agriculture, l'Alimentation et l'Environnement user on 28 April 2023

in early-March for Capriss, Gariguette, Clery and Ciflorette, while they appeared in mid-February for Cir107 and Darselect. Third- and fourth-order modules appeared at the last date of observation (early-June) except for Darselect, for which third-order modules appeared in early-April. The six genotypes also showed marked differences in of flowering intensity, which is reflected in the different sizes of the light blue boxes representing the number of flowers per inflorescence, clearly visible in 3D visualization without leaves (Supplementary Fig. S3). For Gariguette and Cir107, flowering was already intense for all plants in early-March while at this date, flowering started for the four other genotypes.

The 2D representation of the spatio-temporal architecture is represented by the most central plant for each date of the six successive observations (Fig. 4B for Ciflorette; Supplementary Fig. S4 for all genotypes). This representation highlights the succession of incremental order modules (Fig. 4C), the spatio-temporal development of branching, and its variability between genotypes (Supplementary Fig. S4). AXB description was summarized by the stage of its meristem. As an example, along plant development, Ciflorette produced BC in addition to its EC (Figs 4B, C). These branches occurred mainly in the proximal and distal zones of the PC (zeroth-order module). In this zeroth-order, AXB of the median zone were dormant and already initiated at plantation; they did not develop into BC during plant development and dried (rated as aborted). Comparison of 2D architectures between the six genotypes shows that they differ by their complexity and in particular by their branching behavior. This difference in branching leads to different numbers of BC. In early-June, Gariguette showed two apparent axes, while Ciflorette, Clery and Darselect, three, and Capriss and Cir107 four (Supplementary Fig. S4). In addition, distribution of BC along the zeroth-order module differed between genotypes, the three of Capriss and Cir107 being distributed from the bottom to the top while the single ones of Gariguette were at the top. However, the six genotypes were very similar with respect to the fate of the AXB localized on the median zone of the zeroth-order since they were almost all initiated at plantation and stayed dormant or aborted during the experiment.

Exploration of the architectural development of strawberry and its genetic modulation

Regardless of their differences, the strawberry genotypes share a common architectural pattern characterized by:

- A zeroth-order module with a far higher number of phytomers (6-10) than the higher-order modules (2-4) (Fig. 5A), the number of phytomers of the modules of order ≥ 1 being roughly constant for most of the genotypes (see the linear trends estimated for the number of phytomers as a function of the order for order ≥ 1 in Supplementary Table S4).
- A terminal inflorescence with a far higher number of flowers for the zeroth-order module (10-18) compared to higher-order modules (Fig. 5B), the number of flowers being most often slightly higher for first-order modules (4-8) compared to modules of order ≥ 2 (4-6) (see the

Accepted Manuscript

Downloaded from https://academic.oup.com/jxb/advance-article/doi/10.1093/jxb/erad097/7143673 by INRAE Institut National de Recherche pour l'Agriculture, l'Alimentation et l'Environnement user on 28 April 2023

linear trends estimated for the number of flowers as a function of the order for order ≥ 2 in Supplementary Table S4).

- The presence of stolons in zeroth-order modules, their absence in first-order modules and their almost absence in second-order modules, then the number of stolons per module increasing with the module order onward (Fig. 5C).

There are quantitative differences between genotypes, these differences being more pronounced for the zeroth-order modules and for flowering intensity (Figs 5A-C). Concerning the vegetative development, the genotypes can be ordered in the following way according to the number of phytomers of the zeroth-order module (Fig. 5A; Supplementary Table S5): {Gariguette, Capriss, Cir107} > {Ciflorette, Clery} > Darselect. Concerning the complexity of the terminal inflorescence, in term of the number of flowers, Gariguette and Cir107 were the genotypes with the most complex inflorescences whatever the module order while Capriss exhibited the least complex inflorescences (Fig. 5B; Supplementary Table S6). For the three other genotypes with intermediate inflorescence complexity (Ciflorette, Clery and Darselect), the complexity varies according to the module order.

Concerning the stolons, the situation is contrasting between zeroth-order modules and modules of order ≥ 3 (Fig. 5C; Supplementary Table S7). For instance, Capriss exhibited the highest number of stolons for the zeroth-order module and the lowest for third-order modules while Ciflorette exhibited an intermediate number of stolons for the zeroth-order module but the highest number of stolons by far for third- and fourth-order modules.

Finally, concerning the number of modules of order ≥ 1, Capriss and Cir107 were the most bushy genotypes with the highest numbers of first- and second-order modules while Gariguette, Clery and Darselect were the less bushy genotypes with the lowest numbers of first- and second-order modules, Ciflorette being intermediate between these two groups (Supplementary Table S3).

To assess the dates of occurrence of successive module orders (Table 1), we used high-quantile criteria (0.9-quantile) that rely on the whole distribution of module order (Supplementary Table S8 for details on the distribution of module order for successive date). We used this approach to take into account the small sample sizes (nine individuals per observation date for each genotype) and the non-robustness of the maximum criterion. It should be noted that the highest module order was relatively homogeneous between individuals of a given genotype for each successive observation date as illustrated by the 3D visualization of individuals in Supplementary Fig. S2. This statistical analysis also revealed differences between the six genotypes with regard to the timing of module orders. At plantation (mid-December), all genotypes were composed of zeroth and first- order modules except Gariguette, for which the first module order occurred one month later (early-January). Second-order modules occurred less than one month later for Cir107 (early-January) and less than two months after for Capriss, Ciflorette and Darselect (mid-February). It is noteworthy that second-order modules occurred late for Clery and Gariguette (mid-March). Third-order modules occurred earlier for Darselect (mid-March) than for the five other genotypes (early-June). At the last

Accepted Manuscript

Downloaded from https://academic.oup.com/jxb/advance-article/doi/10.1093/jxb/erad097/7143673 by INRAE Institut National de Recherche pour l'Agriculture, l'Alimentation et l'Environnement user on 28 April 2023

date of observation, the highest module order was 3 for Capriss and Cir107 and 4 for Gariguette, Clery, Ciflorette and Darselect (Table 1). Overall, these results suggest differences in module occurrence along the culture according to genotypes.

Three well-differentiated successive zones in zeroth-order module based on axillary productions using a mathematical model

The empirical probabilities of the axillary productions were extracted from the observed sequences synchronized from the top or from the base along the zeroth-order module. These empirical probabilities show a proximal stolon zone followed by a FB median zone when extracted from both the base and the top except for Gariguette (Fig. 6; and Supplemental Fig. S5, respectively). A distal short lateral BC zone (always a single phytomer) is observed when empirical probabilities were extracted from the top (Supplementary Fig. S5) but with a lower probability for Darselect (0.35) compare to the five other variety (>0.60) (Table 2). We thus assumed that three well-differentiated successive zones (semi-Markovian states: 0.1, 0.2, 0.3) can be identified in the zeroth-order module until F0 Markovian state (i.e. inflorescence of the zeroth-order module) for all genotypes except Gariguette. For Gariguette, we assumed that only two well-differentiated successive zones could be identified (the three zones assumption was tested but, in this case, the iterative estimation algorithm of the HMSM chain led to two first zones in parallel with rather similar compositions in terms of axillary productions). A HMSM chain was built for each genotype (Ciflorette in Fig. 3 and all genotypes in Supplementary Fig. S6; Tables 2, 3).

A global model was also built on the basis of the pooled sample with three zones for zeroth-order modules from which zone lengths and compositions were extracted for each genotype on the basis of the optimal segmentation in zones (Supplementary Table S9). This global model shows that the three successive zones in zeroth-order modules (proximal stolon zone, median bud zone and distal short BC zone) are reasonably shared by all the genotypes. We obtained high percentages of match between the segmentations in three zones obtained using the global model and the genotype-specific model for all the genotypes (97% to 65.2%; Gariguette was excluded from the analysis). This global model also shows that both the probability of skipping the proximal zone is the highest and the probability of observing stolons in this proximal zone is the lowest for Gariguette (Supplementary Tables S9, S10). This is consistent with the impossibility of identifying this zone on the basis of the sole Gariguette sample.

We also built models with one more zone at the base of zeroth-order modules for Capriss and Cir107 consistently with the high empirical probability of observing a lateral branching at the base of zeroth-order modules for these two genotypes (Supplemental Fig. S5). This short zone was modeled by a Markovian state and confirms the specificity of Capriss and Cir107 regarding this pattern (Supplementary Fig. S7; Supplementary Tables S11) which explains their bushy habit with far more first- and second-order modules compared to the other genotypes (Supplementary Table S3).

Accepted Manuscript

Downloaded from https://academic.oup.com/jxb/advance-article/doi/10.1093/jxb/erad097/7143673 by INRAE Institut National de Recherche pour l'Agriculture, l'Alimentation et l'Environnement user on 28 April 2023

Axillary meristem fate depends on the module order

Higher-order modules were modeled with only one homogeneous zone. We observed and quantified that first and second order modules contain predominantly VB and FB for all genotypes (Supplemental Table S12; Fig. 3A for Ciflorette). From third-order modules, we showed an increase in the proportion of stolons, depending on the genotypes, at the expense of the proportion of FB, as illustrated in Fig. 3A and Supplemental Table S12.

The transition probability evaluated the AXM fate of two successive buds in modules of order superior to zeroth-order (>= 1) (Supplementary Table S13). The probability close to 1 for the transition 'BC → EC' suggests that BC are systematically followed by an EC, in the last phytomer of the module. Moreover, the transition probability leading to stolon (Supplementary Table S14) shows that stolons are rarely preceded by another axillary production in the module order ≥1. In summary, when lateral branching is observed in module orders superior to zeroth-order (86 BC for top modules versus 1053 EC), BC were at the top and stolons were at the base of the module.

Global comparison of genotypes

Dissimilarity measures between models corresponding to succession of modules from zeroth to fourth order estimated for each genotype (Table 2) and between models restricted to zeroth-order modules were computed. The clustering of genotypes (Fig. 7) on the basis of matrix of pairwise dissimilarity measures between models mainly reflects the difference between zeroth-order modules (Table 2):

- Gariguette with no well-defined proximal stolon zone;
- Ciflorette and Clery with the highest proportion of FB in the median bud zone;
- Capriss and Cir107 with far more BC at the base of the zeroth-order module;
- Darselect with few FB in the median zone and few BC in the distal zone.

It should be noted that this clustering is consistent with the ordering of genotypes according to the number of phytomers of the zeroth-order module (Fig. 5; Supplementary Table S5) with {Gariguette,Capriss, Cir107} > {Ciflorette, Clery} > Darselect and with the far more bushy habit of Capriss and Cir107 with respect to the other genotypes (Supplementary Table S3). The 2D schematic representation of most central individuals (Supplementary Fig. S4) highlights the delayed appearance of first-order modules in Gariguette and the more basal branching of Capriss and Cir107, and to a lesser extent of Ciflorette.

Open-source software and web application for 3D visualization and architectural analysis

Three software artifacts (Fig. 2) have been developed for the analysis and visualization of strawberry architectural data and development: i) the *OpenAlea.Strawberry* Python package, ii) a set of interactive Jupyter Notebook tutorials, and iii) an end-user web application. First, *OpenAlea.Strawberry* is an open-source Python package (https://github.com/openalea/strawberry), available in the OpenAlea platform (Pradal *et al.*, 2008, 2015). *OpenAlea.Strawberry* relies mainly on

Accepted Manuscript

Downloaded from https://academic.oup.com/jxb/advance-article/doi/10.1093/jxb/erad097/7143673 by INRAE Institut National de Recherche pour l'Agriculture, l'Alimentation et l'Environnement user on 28 April 2023

Python 3, OpenAlea.PlantGL (Pradal, *et al.*, 2009), and OpenAlea.MTG (Pradal and Godin, 2020). It provides methods for the architecture reconstruction, analysis at the node and module scale, and 2D and 3D visualization. As shown in Fig. 2, it enables to a) load a MTG file format that encodes in a standard way (topology and property) the description of strawberry architectural data and provides a generic and multiscale MTG data structure , b) visualize in 2D and 3D architectural data of one plant, one or several genotypes), c) analyze the architectural data at different scales (i.e. node, module and plant scales) by providing various exploratory functions to plot and extract data for further analysis such as estimation of HMSM models. Second, the Jupyter Notebook tutorials, designed for scientists, provide an interactive web interface to illustrate the various steps of the pipeline and run existing analyses in a reproducible way (Kluyver *et al.*, 2016). The full software and user documentation, including some tutorials, is available and updated after each change (https://strawberry.rtfd.io). Finally, a web application has been designed on the top of the OpenAlea.Strawberry package to automatically visualize and analyze strawberry architecture for end-users such as breeders. A demonstration of the application is provided through a video (see Supplementary Video, https://data.inrae.fr/dataset.xhtml?persistentId=doi:10.57745/XJY5RO). This application is built using Voilà and Jupyter frameworks. The web application can be installed directly from github or using the Docker image (Merkel, 2014) available on DockerHub (https://hub.docker.com/r/openalea/strawberry) for faster deployment.

Discussion

An open-source software and modeling approach to characterize the complex architecture of strawberry

In strawberry as in other crop species, flower and fruit production is highly dependent on plant and inflorescence architecture (Eshed and Lippman, 2019). In addition to yield, the timing and duration of fruit production, which is also related to the architecture of the plant, is an essential trait for strawberry growers and breeders (Hytönen *et al*., 2008; Gaston *et al*., 2013; Perrotte *et al*., 2016; Tenreira *et al*., 2017; Andrés *et al*., 2021). Compared to most other crops, the specificity of strawberry is that AXB apical meristem (AXM) can produce either a branch (lateral or extension axis), a dormant bud (lateral non-extended axis) or a stolon (Savini *et al*., 2006; Costes *et al*., 2014; Fig. 4C). Furthermore, the fate of the AXM depends on its position on the axis, as demonstrated here. An additional level of complexity in strawberry is that acquiring high-resolution plant architecture datasets requires a destructive step, namely dissecting the primary crown (PC), which is a compact structure (Tenreira *et al*., 2017). Powerful tools are thus required to analyze the large and complex datasets produced by phenotyping and to represent the evolution over time of 2D and 3D architectures of plant and inflorescence and their impact on flower and fruit production.

Accepted Manuscript

Downloaded from https://academic.oup.com/jxb/advance-article/doi/10.1093/jxb/erad097/7143673 by INRAE Institut National de Recherche pour l'Agriculture, l'Alimentation et l'Environnement user on 28 April 2023

To address these challenges, we first developed a free and open-source software library and web application, called *OpenAlea.Strawberry*, that allows the analysis of phenotypic traits relevant to strawberry architecture, which include the occurrence of branching modules according to their order, as well as the complexity of inflorescences. By combining 2D and 3D representation of strawberry plant development and exploratory statistical methods, our software enables comprehensive comparison of branching structure and inflorescence complexity in plants from diverse genotypes or under different environmental conditions. Using *OpenAlea.Strawberry*, we could analyze over time the phenotypic variation in plant and inflorescence architecture of six strawberry genotypes that were extensively described monthly at node scale. By considering the spatio-temporal growth of the plant and formally describing plants through Multiscale Tree Graphs (MTG) (Godin and Caraglio, 1998), we were able to highlight and analyze the diversity of the growth strategies used by the various strawberry genotypes to build their architecture.

We then extracted from *OpenAlea.Strawberry* the data needed to build a model to identify homogeneous zones for axillary productions. This model explicitly integrates the local scale of the phytomer and the more macroscopic scale of the branching zone, and allows for the study of spatial and temporal dependencies between different modules (Peyhardi *et al*., 2017). Using the HMSM chain (Guédon, 2005; Guédon *et al*., 2022), we could show that the zeroth-order module (PC) is structured, regardless of genotype (except Gariguette), into three distinct and homogeneous zones with respect to AXM fate. The three zones produce either stolons and BC (basal zone), dormant buds (central zone) or BC (proximal zone). In higher-order modules derived from the extension axis, AXM fate depends on order level, and the proportion of stolons increases with the module order. The increase in the proportion of stolons is likely due to long days (Kurokura *et al*., 2005; Messetani *et al*., 2011; Labadie *et al*., 2019) and/or low apical dominance (Neri *et al.*, 2003). The original data produced by our analyses represent a significant advance over previous studies that did not consider the time scale or dependencies between different modules (Massenati *et al*., 2011; Bosc *et al*., 2012). They further allow comparison with *Rosaceae* tree species, for example apple and apricot, where the axis is structured in consecutive zones homogeneous in their axillary productions (Renton *et al*., 2006; Costes *et al*., 2014; Mészáros *et al*., 2020). In strawberry, *OpenAlea.Strawberry* can be used to study the influence of the environment on the possible fluctuation of the three zones, as shown in apple (Mészáros *et al*., 2020).

The date of occurrence of successive module orders has a major impact on flowering patterns

The power of the approach describing the module orders at spatial and temporal levels (Peyhardi *et al*., 2017) was highlighted by the demonstration that the occurrence of module orders varies according to the genotype. Moreover, the time elapsed between the occurrence of two successive module orders can be more or less extended depending on the genotype (Table 1). By comparing the results from our temporal study of the architecture with the previous phenological analysis carried out on the same trial (Labadie *et al*., 2019), we could further link the occurrence and time elapsed between two successive module orders with the flowering patterns of each of the six genotypes (Fig. 8). In strawberry, the first flush of flowering is mainly produced by the zeroth- and

Accepted Manuscript

Downloaded from https://academic.oup.com/jxb/advance-article/doi/10.1093/jxb/erad097/7143673 by INRAE Institut National de Recherche pour l'Agriculture, l'Alimentation et l'Environnement user on 28 April 2023

first-order modules (Massetani and Neri, 2016; Bosc *et al*., 2012) (Fig. 8). These modules are initiated in the nursery when temperature and day length are reduced (Opstad *et al*., 2011; Heide *et al*., 2013). The resumption of flower production in May for Clery and Gariguette (Labadie *et al*., 2019) takes place approximately two months after the occurrence of the second-order modules (in March), which is consistent with a period of about 9 weeks between floral initiation and inflorescence emergence (Battey *et al*., 1998; Sønteby and Heide, 2008). In the Capriss, Cir107, Ciflorette and Darselect genotypes, the first flush of flowering is not followed by a stop in the appearance of flowers because the flowering of the second-order module takes over very quickly from that of the zeroth- and first-order modules. Our findings have considerable consequences for strawberry breeding, as shortening the intervals between the occurrence of module orders is critical for growers to control the yield and duration of fruit production (Kurokura *et al*., 2005). Indeed, a main goal of growers is to avoid the interruption of the production.

Genetic diversity in shoot branching is likely related to variability in apical dominance

In strawberry, shoot branching plays a central role in controlling fruit yield because each axis is terminated by an inflorescence when the environment is favorable (Kurokura *et al*., 2017; Tenreira *et al*., 2017; Gaston *et al*., 2020; Gaston *et al*., 2021). Our 2D and 3D plant architecture representation indicated the great diversity for this trait among the various genotypes studied, which led to more or less bushy plants (Supplementary Figs S2-S4). Thanks to our HMSM model, we could further show that branching occurs with very high probability in the very short distal zone (a single phytomer) and in the proximal zone. Branching is regulated by apical dominance, which exerts control over axillary bud outgrowth from the shoot apex (Cline, 1997; Barbier *et al*, 2017). Apical dominance is released when the SAM becomes floral or is removed, for example by grazing or pruning, thus allowing axillary buds to grow and new axes to form. In strawberry, an apex excision experiment (Neri *et al*., 2003) showed that lower AXBs, i.e. those corresponding to our basal zone, can develop into BC when the buds are released from apical dominance. As previously suggested by Sugiyama *et al*. (2004) and observed in tomato (Lifschitz and Eshed, 2006), the genetic diversity observed among the six genotypes studied could be due to variability in the capacity of their axillary buds to be released from apical dominance. In the two bushy genotypes Capriss and Cir107, the lower effect of dominance could lead to the specific fourth zone of branching observed in the basal part of the plant (Supplementary Fig. S7; Supplementary Table S11). These findings underline the importance of branching on the zeroth-order module for increasing the number of inflorescences of the plant. They further lay the foundation for breeding new strawberry cultivars with specific branching features adapted to the various patterns of fruit production required by the growers.

The inflorescence complexity dictates the intensity of the first flowering flush

In addition to branching, inflorescence architecture is a key agronomical factor for yield (Eshed and Lippman, 2019; Gaarslev *et al*., 2021; Koppolu *et al*., 2022). In agreement with Guttridge (1955) and Ridout *et al*. (1999), we clearly show that the inflorescences of the zeroth-order module produced more flowers and therefore showed more complex inflorescences. We further demonstrate here

Accepted Manuscript

Downloaded from https://academic.oup.com/jxb/advance-article/doi/10.1093/jxb/erad097/7143673 by INRAE Institut National de Recherche pour l'Agriculture, l'Alimentation et l'Environnement user on 28 April 2023

that there is a sharp decrease of inflorescence complexity on the first-order module, followed by a slower reduction until stabilization in the higher-order modules (Fig. 5). Variations in the inflorescence complexity produced by the first two modules should therefore considerably affect the number of flowers produced by the plant. In agreement with previous findings (Darrow, 1929; Battey *et al*., 1998), we observed that the genetic background has a strong influence on inflorescence architecture. Moreover, of the six varieties studied, the two genotypes with the most complex inflorescences on the zero-order and first-order modules, Gariguette and Cir107, also exhibit the most intense first flush of flowering (Labadie *et al*., 2019) (Fig. 8). This trait is of the utmost importance to growers and constitutes a major breeding target for the control of fruit yield in strawberry. According to our results, breeding programs aimed at controlling the intensity of the first flowering flush should focus on the complexity of the first inflorescences. To translate flowering into fruit production, however, care should be taken to maintain the reproductive success of all flowers (Rindom and Hansen, 1995).

Future directions

The genetic and molecular control of plant and inflorescence architecture has been deciphered in many domesticated crop species such as rice, maize and tomato (Wang and Li, 2006; Liu *et al*., 2013; Park *et al*., 2014a; Gaarslev *et al*., 2021). This knowledge has been widely exploited to increase crop yield (Eshed and Lippman, 2019), for example in tomato, a sympodial fruit-bearing species like strawberry (Gaston *et al*., 2020). In tomato, considerable increase in fruit yield has been achieved through genetic and biotechnological control of branching (Park *et al*., 2014b) and inflorescence complexity (Rodriguez-Leal *et al*., 2017). In strawberry, the plant architecture and thus the trade-off between fruit yield (through flowering) and daughter plant yield (through runners) depends on the fate of the AXM (Tenreira *et al*., 2017; Gaston *et al*., 2020; Gaston *et al*., 2021). The subsequent difficulty of phenotyping and analyzing plant architecture, in particular, has so far prevented progress similar to that in tomato, although significant advances have been made in our understanding of flowering regulation (Kurokura *et al*., 2017; Gaston *et al*., 2021) and AXM fate (Tenreira *et al*., 2017; Caruana *et al*., 2018; Andrés *et al*., 2021; Liang *et al*., 2022).

The free and open-source software library and web application provided here will allow users to analyze phenotypic traits related to strawberry architecture and yield, including the occurrence of modules and complexity of inflorescences. There are numerous directions for applied and basic research. Our tool and strategy described here will prove particularly useful to strawberry breeders for whom controlling yield pattern throughout the production period is essential. Future developments will, for example, use the data extracted from *OpenAlea.Strawberry* to predict the yield of a given strawberry variety based on its architecture and reproductive success. It will also be used to screen genetic resources by genome-wide association study and obtain information on the genetic control of phenotypic traits related to architecture, as well as to analyze the modulation of plant architecture by the environment, for example by light or temperature (Rantanen *et al*., 2014; Ye *et al*., 2021).

Accepted Manuscript

Downloaded from https://academic.oup.com/jxb/advance-article/doi/10.1093/jxb/erad097/7143673 by INRAE Institut National de Recherche pour l'Agriculture, l'Alimentation et l'Environnement user on 28 April 2023

Supplementary Figures

Figure S1. Average temperature and global radiation at Douville in 2014 and 2015.

Figure S2. 3D representation of the 9 plants of the six genotypes.

Figure S3. 3D representation of the 9 plants without leaflets of the six genotypes.

Figure S4. 2D schematic representation of the most central plant of the six genotypes during the seasonal production.

Figure S5. Probabilities of the axillary productions as a function of the node rank for the six varieties.

Figure S6. HMSM chain in three homogeneous zones on the six genotypes for zeroth-order module.

Figure S7. HMSM chain in four homogeneous zones on Capriss and Cir107 for zeroth-order module.

Supplementary Tables

Table S1. Chilling requirement and flowering earliness for the six genotypes.

Table S2. Specification of the MTG for the cultivated strawberry.

Table S3. Characteristics of samples of sequences.

Table S4. Linear trend for the number of phytomers as function of module order for first-order and the number of flowers.

Table S5. Mean number of phytomers and grouping of genotypes using ANOVA.

Table S6. Mean number of flowers and grouping of genotypes using ANOVA.

Table S7. Mean number of stolons and grouping of genotypes using ANOVA.

Table S8. Module order frequency distribution for the six genotypes.

Table S9. Length and axillary productions in the three zones identified by the HMSM model.

Table S10. Probabilities of skipping –proximal (prox.), median (med.) or distal (dist.)– zones.

Table S11. Length and axillary productions in the four zones identified by the HMSM model.

Accepted Manuscript

Downloaded from https://academic.oup.com/jxb/advance-article/doi/10.1093/jxb/erad097/7143673 by INRAE Institut National de Recherche pour l'Agriculture, l'Alimentation et l'Environnement user on 28 April 2023

Table S12. Zone length and axillary productions of the first- to fourth- order modules.

Table S13. Probabilities of transition from a lateral branch crown in modules of order ≥ 1.

Table S14. Probabilities of transition leading to a stolon in modules of order ≥ 1.

Supplementary Video

https://data.inrae.fr/dataset.xhtml?persistentId=doi:10.57745/XJY5RO

Acknowledgements. This paper is dedicated to the memory of our dear co-worker Yann Guédon, who was central to this work and passed away while this paper was being prepared. The authors thank Lauriane Rouan for her constructive advice. We also thank Christian Gauthier and Cédric Duranton from Invenio for strawberry culture and Fabien Barthoulot for help in phenotyping.

Authors contributions

B.D. with contributions of M.L. designed the study; M.L. and K.G. collected the data with inputs from M.-N.D.; C.P. and M.L. designed and implemented the visualization exploratory tools with inputs from G.H. and Y.C.; Y.G. designed the statistical analysis and implemented the statistical models. M.L., C.P. and Y.G. analyzed the data with inputs from B.D. and Y.C.; M.L., C.P., B.D., C.R. and Y.G. wrote the manuscript. M.L., K.G., MN.D., Y.C., G.H., A.G., C.R., Y.G., C.P., B.D. discussed the results and commented on the manuscript.

Conflict of interest. No conflict of interest declared.

Funding. The project was funded by région Nouvelle Aquitaine (AgirClim project N°2018-1R20202), Friendly Fruit, an EIT Climate-KIC project and European Union's Horizon 2020 research and innovation program (GoodBerry project N° 679303; BreedingValue project N° 101000747). ML, CP and YC have been supported by the MaCS4Plants CIRAD network, initiated from the AGAP Institute and AMAP joint research units.

Data availability.

All data are available in Github: https://github.com/openalea/strawberry/tree/master/share/data

Accepted Manuscript

Downloaded from https://academic.oup.com/jxb/advance-article/doi/10.1093/jxb/erad097/7143673 by INRAE Institut National de Recherche pour l'Agriculture, l'Alimentation et l'Environnement user on 28 April 2023

References

Andrés J, Caruana J, Liang J, Samad S, Monfort A, Liu Z, Hytönen T, Koskela EA. 2021. Woodland strawberry axillary bud fate is dictated by a crosstalk of environmental and endogenous factors. *Plant Physiology* **187**, 1221-1234.

Barbier FF, Dun EA, Beveridge CA. 2017. Apical dominance. *Current Biology* **27**, R864–R865.

Barthélémy D, Caraglio Y. 2007. Plant architecture: a dynamic, multilevel and comprehensive approach to plant form, structure and ontogeny. *Annals of Botany* **99**, 375–407.

Barthélémy D, Caraglio Y, Sabatier S. 2009. Crown architecture of valuable broadleaved species. In : Valuable broadleaved forests in Europe. Spiecker Heinrich (ed.), Hein Sebastian (ed.), Makkonen-Spiecker Kaisu (ed.), Thies Michael (ed.). EFI. Leyde : Brill, 87-101. (European Forest Institute Research Report, 22) ISBN 978-90-04-16795-7.

Battey N., Miere P, Tehranifar A, Cekic C. 1998. Genetic and environmental control of flowering in strawberry. In: Gray D, Cockshull KE, Seymore GB, Thomas B, eds. Genetic and environmental manipulation of horticultural crops. Wallingford, UK: CAB International, 111–131.

Bosc JP, Neri D, Massetani F, Bardet A. 2012. Relationship between plant architecture and fruit production of the short-day strawberry cultivar Gariguette. *Journal of Berry Research.* **2**, 105–111.

Chen Y, Dan Z, Gao F, Chen P, Fan F, Li S. 2020. *Rice GROWTH-REGULATING FACTOR7* Modulates Plant Architecture through Regulating GA and Indole-3-Acetic Acid Metabolism. *Plant Physiology* **184**, 393-406.

Caruana JC, Sittmann JW, Wang W, Liu Z. 2018. Suppressor of runnerless encodes a DELLA protein that controls runner formation for asexual reproduction in strawberry. *Molecular Plant* **11**, 230–233.

Cilas C, Bar-Hen A, Montagnon C, Godin C. 2006. Definition of architectural ideotypes for good yield capacity in Coffea canephora. *Annals of Botany* **97**, 405–411.

Cline MG. 1997. Concepts and terminology of apical dominance. *American Journal of Botany* **84**, 1064–1069.

Costes E, Crespel L, Denoyes B, Morel P, Demene M-N, Lauri P-E, Wenden B. 2014. Bud structure, position and fate generate various branching patterns along shoots of closely related Rosaceae species: a review. *Frontiers in Plant Science* **5**, 666.

Darrow GM. 1929. Inflorescence Types of Strawberry Varieties. *American Journal of Botany* **16**, 571–585.

Durand JB, Guédon Y, Caraglio Y, Costes E. 2005. Analysis of the plant architecture via tree-structured statistical models: the hidden Markov tree models. *The New Phytologist* **166**, 813–825.

Ephraim Y, Merhav N. 2002. Hidden Markov processes. IEEE *Transactions on Information Theory* **48**, 1518–1569.

Accepted Manuscript

Downloaded from https://academic.oup.com/jxb/advance-article/doi/10.1093/jxb/erad097/7143673 by INRAE Institut National de Recherche pour l'Agriculture, l'Alimentation et l'Environnement user on 28 April 2023

Eshed Y, Lippman ZB. 2019. Revolutions in agriculture chart a course for targeted breeding of old and new crops. *Science* **366**: eaax0025.

Gaarslev N, Swinnen G, Soyk S. 2021. Meristem transitions and plant architecture-learning from domestication for crop breeding. *Plant Physiology* **187**:1045-1056.

Gaston A, Osorio S, Denoyes B, Rothan C.2020. Applying the Solanaceae Strategies to Strawberry Crop Improvement. *Trends in Plant Science* **25**, 130-140.

Gaston A, Potier A, Alonso M, Sabbadini S, Delmas F, Tenreira T, Cochetel N, Labadie M, Prévost P, Folta KM, Mezzetti B, Hernould M, Rothan C, Denoyes B. 2021. The FveFT2 florigen/FveTFL1 antiflorigen balance is critical for the control of seasonal flowering in strawberry while FveFT3 modulates axillary meristem fate and yield. *The New Phytologist* **232**, 372–387.

Godin C, Caraglio Y. 1998. A multiscale model of plant topological structures. *Journal of Theoretical Biology* **191**, 1–46.

Guédon, Y. 2003. Estimating hidden semi-Markov chains from discrete sequences. *Journal of Computational and Graphical Statistics* **12**, 604–639.

Guédon Y. 2005. Hidden hybrid Markov/semi-Markov chains. *Computational Statistics & Data Analysis* **49**, 663–688.

Guédon Y. 2007. Exploring the state sequence space for hidden Markov and semi-Markov chains. *Computational Statistics and Data Analysis* **51**, 2379-2409.

Guédon Y, Heuret P, Costes E. 2003. Comparison methods for branching and axillary flowering sequences. *Journal of Theoretical Biology* **225**, 301–325.

Guédon Y, Caraglio Y, Granier C, Lauri PÉ, Muller B. 2022. Identifying Developmental Patterns in Structured Plant Phenotyping Data. In: Lucas, M. (eds) Plant Systems Biology. Methods in Molecular Biology, vol 2395. Humana, New York, NY, 199–225.

Guttridge CG. 1955. Observations on the Shoot Growth of the Cultivated Strawberry Plant. *Journal of the Horticultural Science* **30**, 1–11.

Hallé F, Oldeman RAA. 1970. Essai sur l'architecture et la dynamique de croissance des arbres tropicaux, Eds. Masson, 178 p.

Hallé F, Oldeman R. 1970. Essai sur l'architecture et la dynamique de croissance des arbres tropicaux. Paris : Masson, 1970, 192 p. (Monographie de Botanique et de Biologie Végétale ; 6).

Heide OM, Stavang JA, Sønsteby A. 2013. Physiology and genetics of flowering in cultivated and wild strawberries – A review. *Journal of Horticultural Science and Biotechnology* **88**, 1–18.

Hytönen T, Mouhu K, Koivu I, Juntilla O. 2008. Prohexadionecalcium enhances the cropping potential and yield of strawberry. *Journal of Horticultural Science* **73**, 210–215.

Accepted Manuscript

Downloaded from https://academic.oup.com/jxb/advance-article/doi/10.1093/jxb/erad097/7143673 by INRAE Institut National de Recherche pour l'Agriculture, l'Alimentation et l'Environnement user on 28 April 2023

Jahn OL, Dana MN. 1970. Crown and inflorescence development in the strawberry Fragaria ananassa. *American Journal of Botany* **57**, 605-612.

Kluyver T, Ragan-Kelley B, Pérez F, Granger B, Bussonnier M, Frederic J, Kelley K, Hamrick J, Grout J, Corlay S, Ivanov P, Avila D, Abdalla S, Willing C and Jupyter development team. 2016. Jupyter Notebooks – a publishing format for reproducible computational workflows. Loizides, Fernando and Scmidt, Birgit (eds.) In *Positioning and Power in Academic Publishing: Players, Agents and Agendas.* IOS Press. 87-90 .

Koppolu R, Chen S, Schnurbusch T. 2022. Evolution of inflorescence branch modifications in cereal crops. *Current Opinion in Plant Biology* **65**:102168.

Kurokura T., Inava Y, Neri D, Sugiyama N. 2005. A morphological study of the development of the second inflorescences in strawberry (Fragaria×ananassa Duch.). *Annals of Applied Biology* **146,** 511–515.

Kurokura T, Samad S, Koskela E, Mouhu K, Hytönen T. 2017. Fragaria vesca CONSTANS controls photoperiodic flowering and vegetative development. *Journal of Experimental Botany* **68**, 4839-4850.

L**abadie M, Denoyes B, Guédon Y. 2019.** Identifying phenological phases in strawberry using multiple change-point models. *Journal of Experimental Botany* **70**, 5687–5701.

Li Y, Hu J, Wei H, Jeong BR. 2020. A Long-Day Photoperiod and 6-Benzyladenine Promote Runner Formation through Upregulation of Soluble Sugar Content in Strawberry. *International Journal of Molecular Sciences* **21**, 4917.

Liang J, Wu Z, Zheng J, Koskela EA, Fan L, Fan G, Gao D, Dong Z, Hou S, Feng Z, Wang F, Hytönen T, Wang H. 2022. The GATA factor HANABA TARANU promotes runner formation by regulating axillary bud initiation and outgrowth in cultivated strawberry. *Plant Journal* **110**, 1237-1254.

Lifschitz E, Eshed Y. 2006. Universal florigenic signals triggered by FT homologues regulate growth and flowering cycles in perennial day-neutral tomato. *Journal of Experimental Botany* **57**, 3405-3414.

Liu C, Teo ZWN, Bi Y, Song S, Xi W, Yang X, Yin Z, Yu H. 2013. A conserved Genetic Pathway Determines Inflorescence Architecture in Arabidopsis and Rice. *Developmental Cell* **24**, 612–622

Massetani F, Gangatharan R, Neri D. 2011. Plant architecture of Strawberry in Relation to Abiotic Stress, Nutriment Application and Type of Propagation System. *Genes, Genomes and Genomics* **5**, 12–23.

Massetani, F. and Neri, D. 2016. Strawberry plant architecture in different cultivation systems. *Acta Horticulturae* **1117**, 291-296.

Mathan J, Bhattacharya J, Ranjan A. 2016. Enhancing crop yield by optimizing plant developmental features. *Development* **143**, 3283-3294.

Merkel. 2014. Docker: lightweight linux containers for consistent development and deployment. *Linux Journal* **239**, 2.

Accepted Manuscript

Downloaded from https://academic.oup.com/jxb/advance-article/doi/10.1093/jxb/erad097/7143673 by INRAE Institut National de Recherche pour l'Agriculture, l'Alimentation et l'Environnement user on 28 April 2023

Mészáros M, Guédon Y, Krška B, Costes E. 2020. Modelling the bearing and branching behaviors of 1-year-old shoots in apricot genotypes. *PLoS One* **15**, e0235347.

Neri D, Sugiyama N, Iwama T, Akagi H. 2003. Effect of Apical Pinching on the Development of Axillary Buds in Strawberry Plants. *Journal of The Japanese Society for Horticultural Science* **72**, 389-392.

Nicolini E, Caraglio Y, Pelissier R, Leroy C, Roggy JC. 2003. Epicormic branches: a growth indicator for the tropical forest tree, Dicorynia guianensis Amshoff (Caesalpiniaceae). *Annals of Botany* **92**, 97-105.

Opstad N, Sønsteby A, Myrheim U, Heide OM. 2011. Seasonal timing of floral initiation in strawberry: effects of cultivar and geographic location. *Scientia Horticulturae* **129**, 127–134.

Park SJ, Eshed Y, Lippman ZB. 2014a. Meristem maturation and inflorescence architecture--lessons from the Solanaceae. *Current Opinion in Plant Biology* **17**, 70-77.

Park SJ, Jiang K, Tal L, Yichie Y, Gar O, Zamir D, Eshed Y, Lippman ZB. 2014b. Optimization of crop productivity in tomato using induced mutations in the florigen pathway. *Nature Genetics* **46**, 1337-1342.

Peyhardi J, Caraglio Y, Costes E, Lauri P-É, Trottier C, Guédon Y. 2017. Integrative models for joint analysis of shoot growth and branching patterns. *The New Phytologist* **216**, 1291–1304.

Perrotte J, Gaston A, Potier A, Petit A, Rothan C, Denoyes B. 2016. Narrowing down the single homoeologous FaPFRU locus controlling flowering in cultivated octoploid strawberry using a selective mapping strategy. *Plant Biotechnology Journal* **14**, 2176–2189.

Pradal, C, Dufour-Kowalski S, Boudon F, Fournier C, Godin C. 2008. OpenAlea: a visual programming and component-based software platform for plant modelling. *Functional Plant Biology* **35**, 751–760.

Pradal C, Boudon F, Nouguier C, Chopard J, Godin C 2009. PlantGL: a Python-based geometric library for 3D plant modelling at different scales. *Graphical models* ***71***, 1-21.

Pradal C, Fournier C, Valduriez P, Cohen-Boulakia S. 2015. OpenAlea: scientific workflows combining data analysis and simulation. In *Proceedings of the 27th International Conference on Scientific and Statistical Database Management,* 1-6.

Pradal C, Godin C. 2020. MTG as a standard representation of plants in FSPMs. In: Book of abstracts of the 9th International Conference on Functional-Structural Plant Models: FSPM2020, 5–9 October, 2020. Germany: University of Hannover. https://hal.inria.fr/hal-03059523/file/abstract7.pdf

Rantanen M, Kurokura T, Mouhu K, Pinho P, Tetri E, Halonen L, Palonen P, Elomaa P, Hytönen T. 2014. Light quality regulates flowering in FvFT1/FvTFL1 dependent manner in the woodland strawberry Fragaria vesca. *Frontiers in Plant Science* **5**, 271.

Reinhardt D, Kuhlemeier C. 2002. Plant architecture. *EMBO Reports* **3**, 846-851.

Accepted Manuscript

Downloaded from https://academic.oup.com/jxb/advance-article/doi/10.1093/jxb/erad097/7143673 by INRAE Institut National de Recherche pour l'Agriculture, l'Alimentation et l'Environnement user on 28 April 2023

Renton M, Guédon Y, Godin C, Costes E. 2006. Similarities and gradients in growth-unit branching patterns during ontogeny in 'Fuji' apple trees: A stochastic approach. *Journal of Experimental Botany* **57**, 3131–3143.

Ridout, Martin S., Morgan, Byron J. T., Taylor, David R. 1999. Modelling variability in the branching structure of strawberry inflorescences. *Journal of the Royal Statistical Society: Series C (Applied Statistics)* **48**, 185-196.

Rindom A, Hansen P. 1995. Effects of fruit numbers and plant status on fruit size in the strawberry. *Acta Agriculturae Scandinavica, Section B — Soil and Plant Science* **45**, 142-147.

Rodríguez-Leal D, Lemmon ZH, Man J, Bartlett ME, Lippman ZB. 2017. Engineering Quantitative Trait Variation for Crop Improvement by Genome Editing. *Cell* **171** 470-480.e8.

Safaa N, Vercambre G, Pagès L, Grasselly D, Gautier H, Génard M. 2009. Tomato plant architecture as affected by salinity: Descriptive analysis and integration in a 3-D simulation model. *Botany* **87**, 893-904.

Savini G, Neri D, Zucconi F, Sugiyama N. 2006. Strawberry Growth and Flowering. International *Journal of Fruit Science* **5**, 29–50.

Schmitz G, Theres K. 1999. Genetic control of branching in Arabidopsis and tomato. *Current Opinion in Plant Biology* **2**, 51-55.

Sønsteby A, Heide OM. 2008. Temperature responses, flowering and fruit yield of the June-bearing strawberry cultivars Florence, Frida and Korona. *Scientia Horticulturae* **119**, 49–54.

Sugiyama N, Iwama T, Inaba Y, Kurokura T, Neri D. 2004. Varietal differences in the formation of branch crowns in strawberry plants. *Journal of the Japanese Society for Horticultural Science* **73**, 216–220.

Teichmann T, Muhr M. 2015. Shaping plant architecture. *Frontiers in Plant Science* **6**, 233.

Tenreira T, Pimenta Lange MJ, Lange T, Bres C, Labadie M, Monfort A, Hernould M, Rothan C, Denoyes B. 2017. A Specific Gibberellin 20-oxidase Dictates the Flowering-Runnering Decision in Diploid Strawberry. *The Plant Cell* **29**, 2168–2182.

Wang Y, Li J. 2006. Genes controlling plant architecture. Current Opinion in Biotechnology. **17**, 123–129.

Ye Y, Liu Y, Li X, Chen Q, Zhang Y, Luo Y, Liu Z, Wang Y, Lin Y, Zhang Y, Wang X, Tang H. 2021. Transcriptome Profile Analysis of Strawberry Leaves Reveals Flowering Regulation under Blue Light Treatment. *International Journal of Genomics* 5572076.

Accepted Manuscript

Downloaded from https://academic.oup.com/jxb/advance-article/doi/10.1093/jxb/erad097/7143673 by INRAE Institut National de Recherche pour l'Agriculture, l'Alimentation et l'Environnement user on 28 April 2023

Tables

Table 1. Occurrence of module order for each genotype and successive dates of observation. The highest module order was extracted from the frequency distribution of module orders with quantile 0.9.

	Capriss	Ciflorette	Cir107	Clery	Darselect	Gariguette
mid-Dec.	1	1	1	1	1	0
early-Jan.	1	1	2	1	1	1
mid-Feb.	2	2	2	1	2	1
early-Mar.	2	2	2	2	3	2
early-Apr.	2	2	2	2	3	2
early-June	3	3&4	3	3&4	4	3&4

Colors of module order correspond to the ones used in the 3D representation of Fig. 3A.

Accepted Manuscript

Downloaded from https://academic.oup.com/jxb/advance-article/doi/10.1093/jxb/erad097/7143673 by INRAE Institut National de Recherche pour l'Agriculture, l'Alimentation et l'Environnement user on 28 April 2023

Table 2. Proximal, median and distal zones of the zeroth-order module for the six genotypes: lengths (number of leaves) and axillary productions (in percentage). Axillary productions were axillary buds (AXB) determined by the developmental stage of their AXM (AB: aborted bud, VB: vegetative bud, IB: initiated bud, FB: floral bud), stolon (ST) or lateral branch crown (BC).

	Proximal zone							Median zone							Distal zone						
		Axillary productions							Axillary productions							Axillary productions					
	Mean	AXB				ST	BC	Mean	AXB				ST	BC	Mean	AXB				ST	BC
	length	AB	VB	IB	FB			length	AB	VB	IB	FB			length	AB	VB	IB	FB		
Gariguette								9	0.1	0.11	0.05	0.6	0.08	0.06	1.1				0.37		0.63
Ciflorette	3.3	0.18	0.02		0.12	0.4	0.28	3.9	0.06	0.08	0.06	0.78		0.02	1				0.27		0.73
Clery	3.5	0.24	0.03		0.13	0.49	0.11	5.1	0.04	0.17	0.08	0.7		0.01	1				0.19		0.81
Capriss	4.9	0.06		0.01	0.12	0.4	0.41	4.1	0.16	0.16	0.13	0.47		0.08	1	0.04			0.3		0.66
Cir107	4.2	0.04			0.11	0.52	0.33	5.7	0.2	0.06	0.01	0.62		0.11	1				0.02		0.98
Darselect	3.4	0.03	0.15		0.23	0.42	0.17	4.2	0.32	0.25	0.07	0.27	0.02	0.07	1	0.13		0.1	0.42		0.35

Accepted Manuscript

https://academic.oup.com/jxb/advance-article/doi/10.1093/jxb/erad097/7143673 by INRAE Institut National de Recherche pour l'Agriculture, l'Alimentation et l'Environnement

Table 3. Probabilities of skipping –proximal (prox.), median (med.) or distal (dist.)– zones in zeroth-order modules

	Prox.	Prox. + med.	Med.	Dist.	Med. + dist.
Gariguette					
Ciflorette	0.17				0.15
Clery	0.01	0.04	0.23		0.07
Capriss					0.02
Cir107	0.08	0.09			0.05
Darselect	0.36				0.62

Empty cells: For Gariguette, the proximal zone does not exist; otherwise, the probability is zero.

Accepted Manuscript

https://academic.oup.com/jxb/advance-article/doi/10.1093/jxb/erad097/7143673 by INRAE Institut National de Recherche pour l'Agriculture, l'Alimentation et l'Environnement

Figure 1

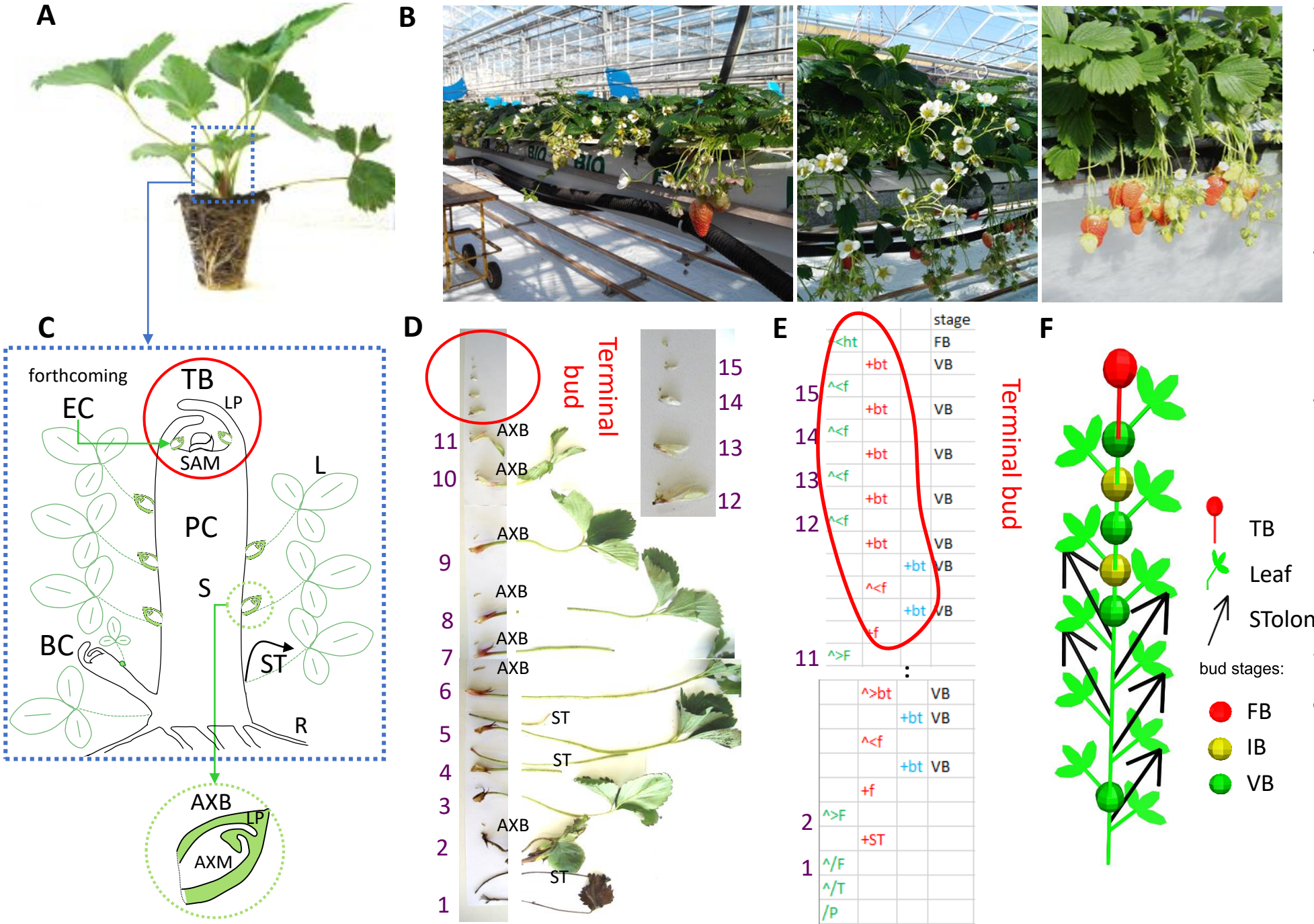

emic.oup.com/jxb/advance-article/doi/10.1093/jxb/erad097/7143673 by INRAE Institut National de Recherche pour l'Agriculture, l'Alimentation et l'Environ

Figure 1: Tree-structured representation of a strawberry plant at plantation.
(A) Tray plant at plantation.
(B) Soilless culture of strawberry in a glasshouse with a focus on flowering and fruiting plants.
(C) Schematic representation of a primary crown (PC). PC includes stem (S), terminal bud (TB) and leaves with their axillary buds (AXB), which are dormant buds (non-extended lateral axes). A lateral branch crown (BC) is also represented. TB includes SAM and leaf primordia (LP). The uppermost AXB will produce the extension crown (EC). Vegetative AXB includes AXM and LP. L, leaf. ST, stolon. R, root.
(D) Dissection of the plant with leaf order according to the rank of the node (numbered from 1 to 15). In the grey rectangle on the left, the leaves with either stolon or AXB at their base. In the grey rectangle on the right, detail of the dissection of the TB.
(E) MTG formalism of the plant with stage property. Colors represent the module order: green for order 0, red for order 1 and blue for order 2. Botanical entities as named in MTG: F, leaf; f, leaf primordium (leaf enclosed in the bud); ST, stolon; BT, bud; ht, inflorescence enclosed in BT; HT: visible inflorescence (not represented in this plant); FB: Floral Bud; VB: Vegetative Bud. '+' indicates a branching link and '< ' a succession link.
(F) 2D schematic representation of the plant generated by the OpenAlea.Strawberry package. Only the PC (zeroth-order module) is represented. The colored spheres indicate the non-visible/undeveloped higher-order modules (starting with "f") of the AXB, as determined by the developmental stage of the AXM. TB: Terminal Bud; FB: Floral Bud; IB: Initiated Bud; VB: Vegetative Bud.

emic.oup.com/jxb/advance-article/doi/10.1093/jxb/erad097/7143673 by INRAE Institut National de Recherche pour l'Agriculture, l'Alimentation et l'Environ

An end-to-end Strawberry Architectural Analysis Pipeline

Figure 2

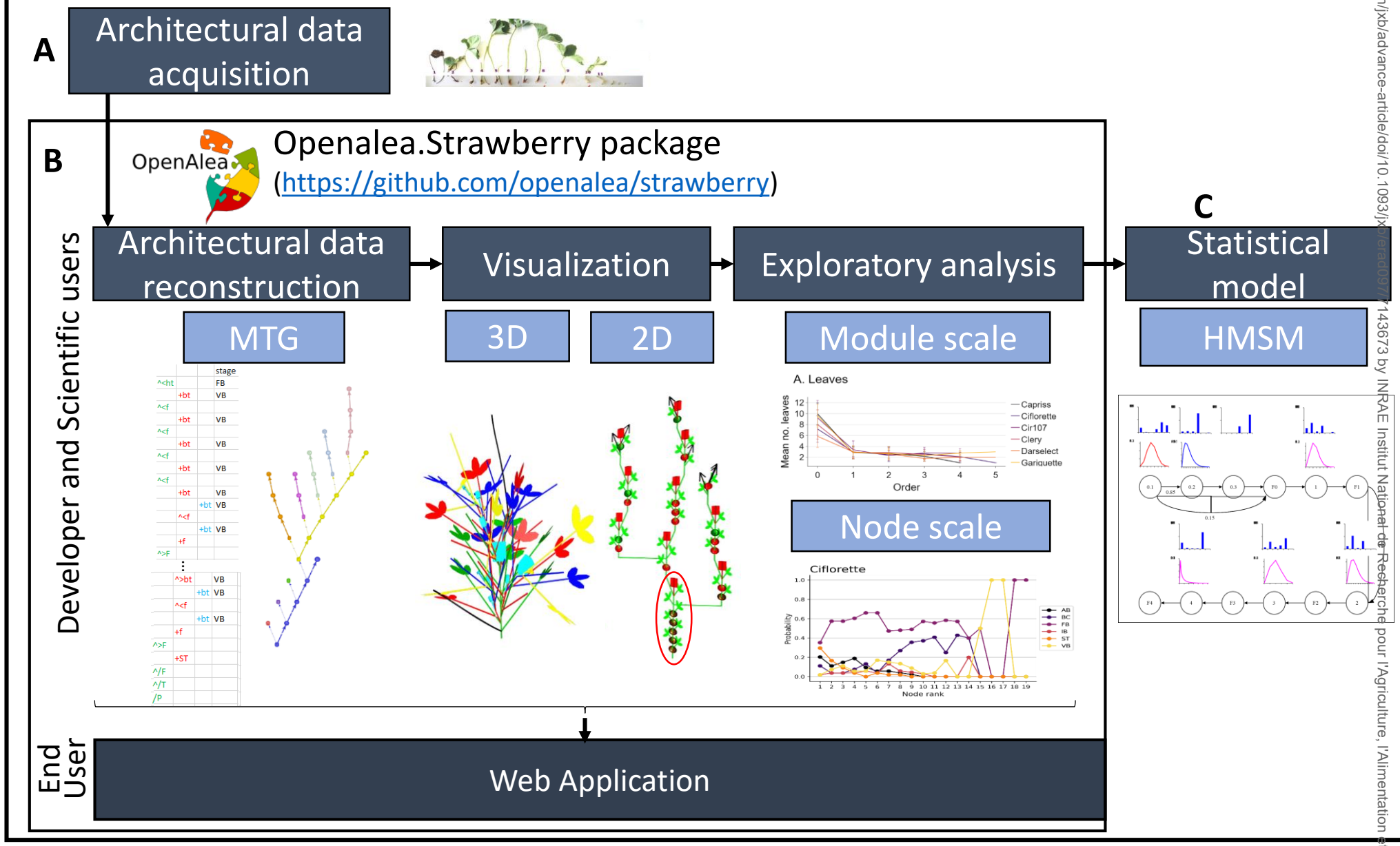

emic.oup.com/jxb/advance-article/doi/10.1093/jxb/erad097/7143673 by INRAE Institut National de Recherche pour l'Agriculture, l'Alimentation et l'Environ

Figure 2. An end-to-end pipeline for the architectural analysis of strawberry with the *OpenAlea.strawberry* package developed in Python on the OpenAlea platform

(A) Architectural data from the strawberry plants were acquired after dissection. Production of axillary buds and the stage of all terminal meristems were described.

(B) Data were transposed in MTG formalism. The pipeline allows users to visualize architectural data in 3D and 2D and explore data at different scales: plant, module or node scale. In the 2D visualisation, an example of module (here the zero-order module) composed of a succession of phytomers is surrounded by red. The succession of modules is represented by a diagonal division between the modules at an angle of 30°, while the branching is represented by a horizontal division at an angle of 90°. TB: Terminal Bud; FB: Floral Bud; IB: Initiated Bud; VB: Vegetative Bud; BC: Lateral Branch Crown; ST, Stolon.

(C) In addition to the strawberry package, a statistical Markov analysis model (HMSM model) was developed to characterize homogeneous zones of axillary productions along apparent axes .

emic.oup.com/jxb/advance-article/doi/10.1093/jxb/erad097/7143673 by INRAE Institut National de Recherche pour l'Agriculture, l'Alimentation et l'Enviror

Figure 3

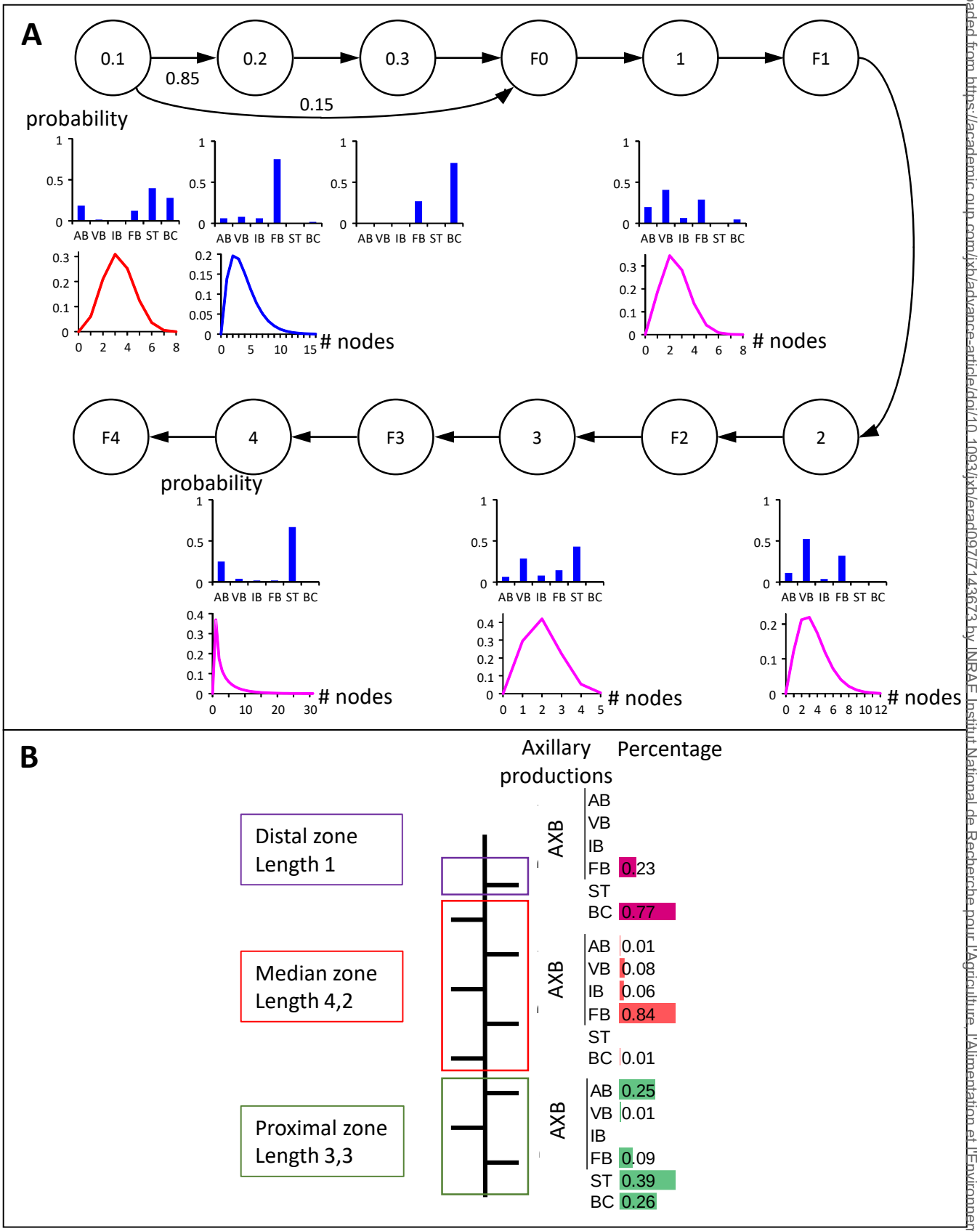

Downloaded from https://academic.oup.com/jxb/advance-article/doi/10.1093/jxb/erad097/7143673 by INRAE Institut National de Recherche pour l'Agriculture, l'Alimentation et l'Environnement user on 28 April 2023

Figure 3. Schematic representations of the Hidden hybrid Markov/semi-Markov chain estimated for Ciflorette.

(A) Hidden Hybrid Markov/semi-Markov chain and its parameters values. Each vertex represents either a Markovian or a semi-Markovian state. Markovian states correspond to terminal inflorescences with their module orders (states F0, F1, F2, F3 and F4). Semi-Markovian states represent zones within the zeroth-order module (0.1: proximal zone, 0.2: median zone, 0.3: distal zone) and module orders (1,2,3,4). Transition probabilities are represented by arrows between states (edge). Transition probabilities are noted nearby when < 1. The observation distributions which represent the zone composition (proportions of axillary productions) and the occupancy distributions which represent the zone length in number of nodes are attached to each state and are at the bottom of the corresponding vertex. For zone composition: x-axis: AB: aborted bud, VB: vegetative bud, IB: initiated bud, FB: floral bud), stolon (ST) or lateral branch crown (BC); y-axis: probability mass. For occupancy distribution: x-axis: number of successive nodes (# nodes); y-axis: probability mass.

(B) Hidden hybrid Markov/semi-Markov summarized on plant architecture for zeroth-order module. Each zone is represented by a color box: green for proximal zone, red for median zone, and purple for distal zone. Each zone was characterized by the mean length zone (mean no. phytomers) and the non-generated observation distribution of axillary productions (in percentage) indicated and colored in data bars. Axillary productions were axillary buds (AXB) determined by the developmental stage of their AXM (AB: aborted bud, VB: vegetative bud, IB: initiated bud, FB: floral bud), stolon (ST) or lateral branch crown (BC).

Downloaded from https://academic.oup.com/jxb/advance-article/doi/10.1093/jxb/erad097/7143673 by INRAE Institut National de Recherche pour l'Agriculture, l'Alimentation et l'Environnement user on 28 April 2023

Figure 4

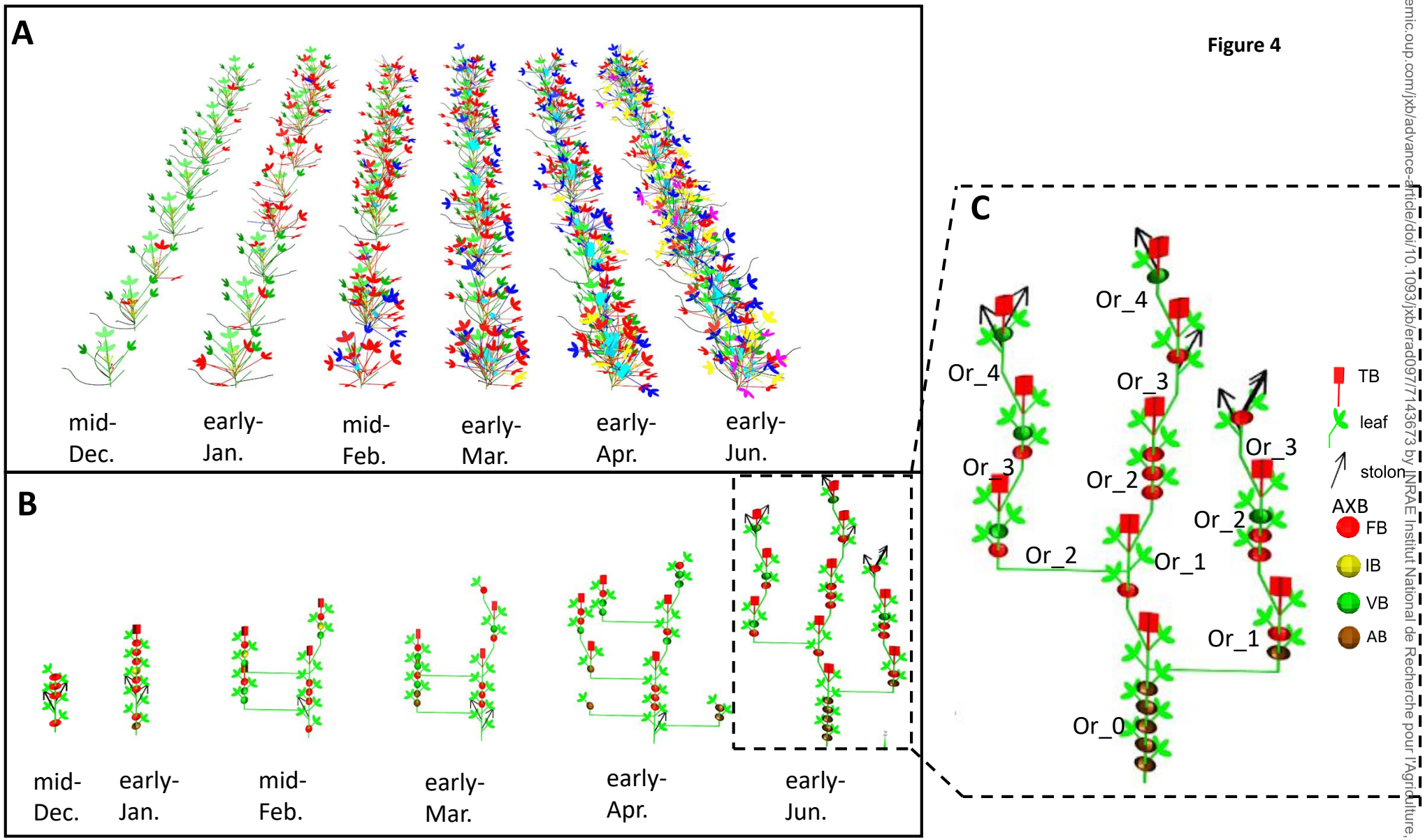

emic.oup.com/jxb/advance-article/doi/10.1093/jxb/erad097/7143673 by INRAE Institut National de Recherche pour l'Agriculture, l'Alimentation et l'Environ

Figure 4. Spatio-temporal architecture of strawberry plant using 3D and 2D representations.
(A) 3D representation of the 9 plants of the genotype Ciflorette during the seasonal production. The seasonal production is represented by six successive dates of observation. Colors represent module orders: green for order 0, red for order 1, blue for order 2, yellow for order 3, and purple for order 4. The size of the light blue boxes representing the inflorescence is proportional to the number of open flowers.
(B) 2D representation of the genotype Ciflorette during the seasonal production. The spatio-temporal architecture of Ciflorette is summarized by the representation of the most central individual for each date of observation. The representation of the development of a given genotype is discontinuous between two dates because the acquisition of the architecture require dissection and is destructive. At each date, a new plant of the same genotype is represented. Each organ is represented by a geometrical shape: inflorescence, red box; phytomer (internode + petiole + 3 leaflets), green cylinder terminated by three green discs; stolon, black arrow; axillary bud (AXB), a sphere colored according to the stage of the terminal meristem (green, yellow, red or brown for respectively vegetative, initiated, floral or aborted/dried stage). Lateral branch crown and extension crown are represented by horizontal or oblique shifts respectively. Apparent axes are materialized by the succession of extension module order from zeroth-order module or from a lateral branch crown.
(C) 2D representation of the most central plant of the genotype Ciflorette at the last date of observation. Module order rank is indicated by the number on the side of each module. At this last observation date, the dry dormant buds observed were considered as aborted buds. They were mainly located on the zero-order module.

emic.oup.com/jxb/advance-article/doi/10.1093/jxb/erad097/7143673 by INRAE Institut National de Recherche pour l'Agriculture, l'Alimentation et l'Enviror

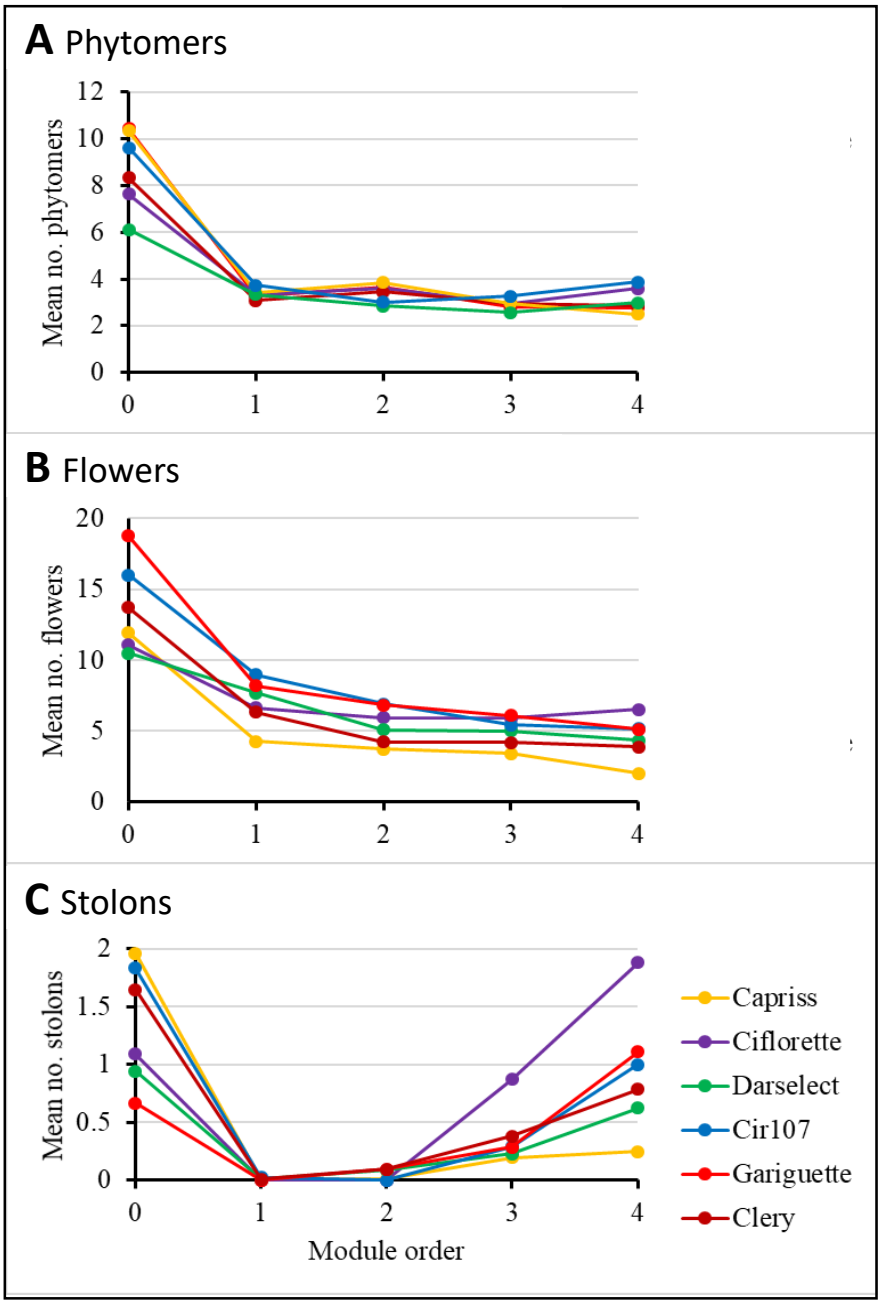

Figure 5. Mean number of (A) phytomers, (B) flowers, (C) stolons as function of module order for each of the six genotypes. Data represent means of 9 plants per genotype.

Downloaded from https://academic.oup.com/jxb/advance-article/doi/10.1093/jxb/erad097/7143673 by INRAE Institut National de Recherche pour l'Agriculture, l'Alimentation et l'Environnement user on 28 April 2023

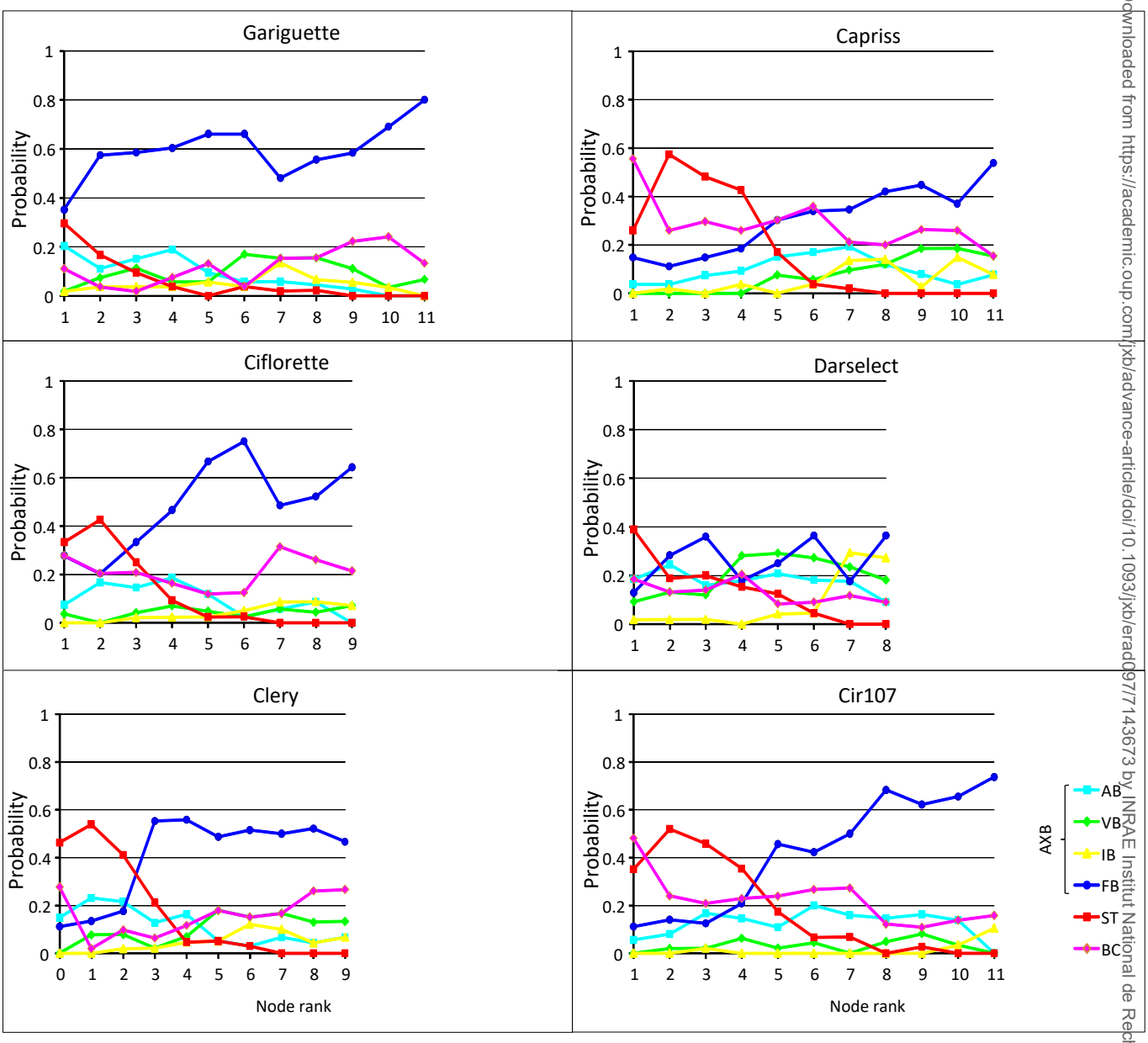

Figure 6. Probabilities of the axillary productions as a function of the node rank for Gariguette, Ciflorette, Clery, Capriss, Darselect and Cir107. The node rank is ordered from the base to the top of the zeroth-order module without the last node bearing the extension crown. Axillary productions were axillary buds (AXB) determined by the developmental stage of their AXM (AB: aborted bud, VB: vegetative bud, IB: initiated bud, FB: floral bud), stolon (ST) or lateral branch crown (BC).

Downloaded from https://academic.oup.com/jxb/advance-article/doi/10.1093/jxb/erad097/7143673 by INRAE Institut National de Recherche pour l'Agriculture, l'Alimentation et l'Environnement user on 28 April 2023

Figure 7

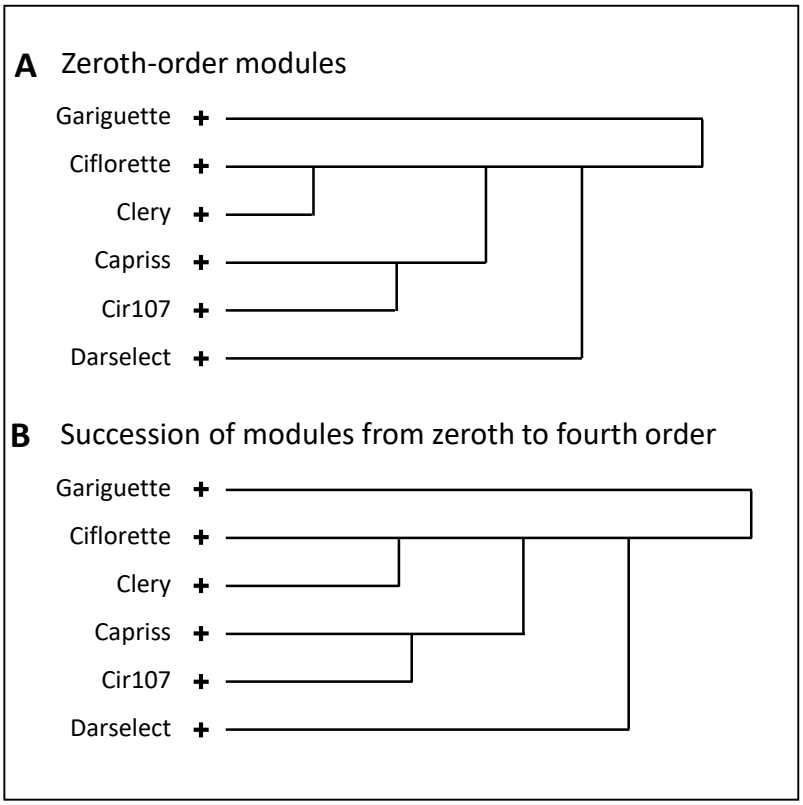

Figure 7. Hierarchical clustering dendrogram of axillary production patterns of the six varieties on the basis of matrix of pairwise dissimilarity measures between models. The matrix of pairwise dissimilarity was calculated on the basis of Kullback-Leibler divergences between estimated hybrid hidden Markov/semi-Markov chains for (A) zeroth-order modules and (B) succession of modules from zeroth to fourth order. The length of the edge between two genotypes in each dendrogram represent the distance or dissimilarity between these genotypes. The sign + indicates the terminal node of the clustering tree.

Downloaded from https://academic.oup.com/jxb/advance-article/doi/10.1093/jxb/erad097/7143673 by INRAE Institut National de Recherche pour l'Agriculture, l'Alimentation et l'Environnement user on 28 April 2023

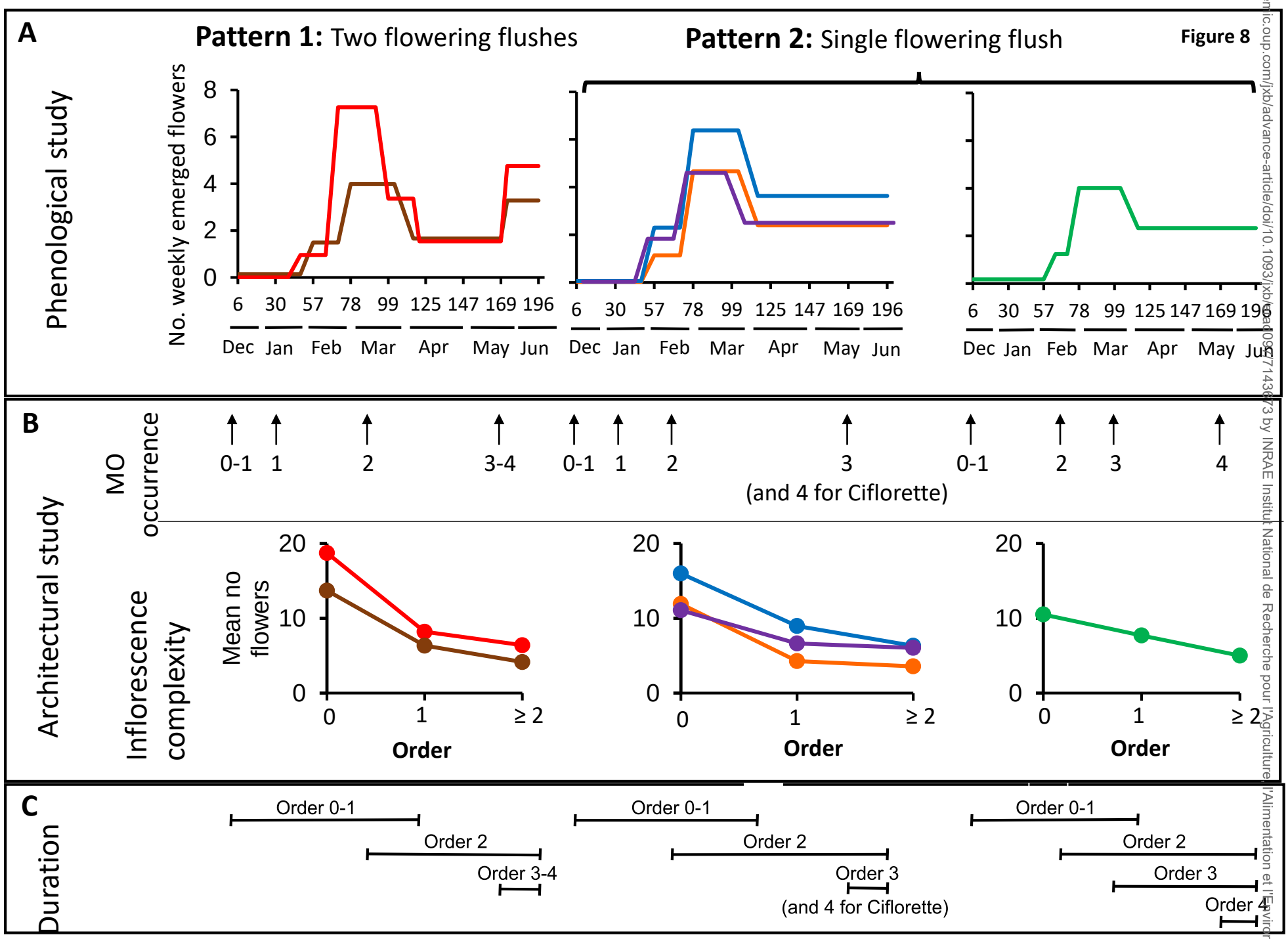

emic.oup.com/jxb/advance-article/doi/10.1093/jxb/eac095/6571436 by INRAE Institut National de Recherche pour l'Agriculture, l'Alimentation et l'Environ

Figure 8: Relationships between flowering phenological phases and architectural data.
(A) Phenological phases were identified using a longitudinal data modeling approach, which highlighted two patterns of flowering: two flushes separated by a phase of lower flower production (pattern 1) or a single flush (pattern 2). Flowering intensity was dependent on genotype. Calendar days and months are indicated in the axis-x.
(B) Architectural study with module order occurrence identified by quantile 0.9 and inflorescence complexity (flower numbers per inflorescence according to the module order).
(C) Duration of the flowering period according to the module order.
Altogether, these results show that the intensity of flower production for the first flush is related to the complexity of the inflorescence at the zeroth and first-order modules. The presence of a near-stop of flowering in genotypes displaying the pattern 1 can be explained by a delay in the occurrence of the second-order module. The absence of flowering stop after the first flush in genotypes displaying the pattern 2 may be due either to the rapid relay of second-order modules for flowering, or to a higher production of lateral branch crowns.

emic.oup.com/jxb/advance-article/doi/10.1093/jxb/erad097/7143673 by INRAE Institut National de Recherche pour l'Agriculture, l'Alimentation et l'Enviror